Mathematical modeling of uniform CO_2 corrosion

34

Aria Kahyarian [1], *Mohsen Achour* [2] *and Srdjan Nesic* [1]
[1]Ohio University, Athens, OH, United States; [2]ConocoPhillips, Bartlesville, OK, United States

34.1 Introduction

Developing more accurate and reliable corrosion rate—predictive tools, specifically for oil and gas industry applications, has been the main objective of many research studies in last few decades. The significance of the predicted corrosion rate in defining the design life of an industrial infrastructure with all the associated health, safety, environmental, and financial concerns, has been a strong driving force for developing better understanding of the corrosion phenomena and advancements in the corrosion rate—predictive tools.

CO_2 corrosion rate—predictive models have undergone a long journey from the initial simplistic nomograms developed in the 1970s [1] to the comprehensive and elaborate mechanistic mathematical models that are now available in the open literature [2]. The progressive development of the ever more capable predictive models was a response to the industrial demands for more accurate corrosion rate predictions. The modern mechanistic models have also become a platform on which it is possible to implement the continuously advancing understandings of the underlying corrosion mechanisms of CO_2 corrosion and illustrate how all the "pieces of the puzzle" fit together to describe the overall process.

The text below is focused on the mathematical models of the CO_2 corrosion of steel (the so-called *sweet* corrosion) as the most common type of internal pipeline corrosion in the oil and gas industry. Even though CO_2 corrosion is almost always observed in transmission pipelines, it is often complicated by the presence of other corrosive species such as organic acids and hydrogen sulfide (aka *sour* corrosion). The detailed discussion of sour corrosion models is beyond the scope of the present article; however, the comprehensive modeling approach described in this chapter for the sweet corrosion can be extended to cover sour corrosion as well as organic acids with slight modifications.

The CO_2 corrosion can be defined as an undesired spontaneous conversion of the iron $Fe_{(s)}$ from steel to its chemically more stable aqueous form $\left(Fe^{2+}_{(aq)}\right)$, where the presence of CO_2 plays an accelerating role. The overall process may be expressed in term of a net redox reaction (34.1).

$$Fe_{(s)} + CO_{2(g)} + H_2O_{(l)} \rightarrow Fe^{2+}_{(aq)} + CO^{2-}_{3(aq)} + H_{2(g)} \tag{34.1}$$

The reaction above summarizes a number of chemical and electrochemical reactions that occur simultaneously, as briefly described below.

Trends in Oil and Gas Corrosion Research and Technologies. http://dx.doi.org/10.1016/B978-0-08-101105-8.00034-6

Table 34.1 Chemical equilibria of dissolved CO_2 in acidic aqueous solutions

$$CO_{2(g)} \rightleftharpoons CO_{2(aq)} \tag{34.2}$$

$$CO_{2(aq)} + H_2O_{(l)} \rightleftharpoons H_2CO_{3(aq)} \tag{34.3}$$

$$H_2CO_{3(aq)} \rightleftharpoons HCO^-_{3(aq)} + H^+_{(aq)} \tag{34.4}$$

$$HCO^-_{3(aq)} \rightleftharpoons CO^{2-}_{3(aq)} + H^+_{(aq)} \tag{34.5}$$

$$H_2O_{(l)} \rightleftharpoons OH^-_{(aq)} + H^+_{(aq)} \tag{34.6}$$

The relevant chemical reactions are the result of CO_2 dissolution in water. Although dissolved CO_2 is not a corrosive species, it leads to acidification of the aqueous solution. The dissolution of CO_2 in water is accompanied by series of homogenous chemical reactions as listed in Table 34.1, giving rise to chemical species such as H^+, H_2CO_3, HCO_3^-, which are known to be electrochemically reactive.

As a heterogeneous process, the corrosion of steel is a result of a number of spontaneous electrochemical reactions occurring simultaneously at the metal surface. Specifically, the cause of metal loss is the anodic oxidation of iron as described via "half-reaction" (34.7), which results in dissolution of solid iron into the aqueous phase and release of electrons. The produced electrons are consumed by simultaneous cathodic (reduction) reactions, keeping the process going. The cathodic "half reactions," commonly associated with CO_2 corrosion, are listed in Table 34.2. The main

Table 34.2 Electrochemical redox reactions associated with CO_2 corrosion of mild steel

Electrochemical reaction	
$Fe^{2+}_{(aq)} + 2e^- \leftarrow Fe_{(s)}$	(34.7)
$H^+_{(aq)} + e^- \rightarrow \frac{1}{2}H_{2(g)}$	(34.8)
$H_2O_{(l)} + e^- \rightarrow OH^-_{(aq)} + \frac{1}{2}H_{2(g)}$	(34.9)
$H_2CO_{3(aq)} + e^- \rightarrow HCO^-_{3(aq)} + \frac{1}{2}H_{2(g)}$	(34.10)
$HCO^-_{3(aq)} + e^- \rightarrow CO^{2-}_{3(aq)} + \frac{1}{2}H_{2(g)}$	(34.11)

electroactive (corrosive) species are H^+, H_2CO_3, HCO_3^-, and H_2O, while their relative importance debated and defined by researchers over the past few decades [3–12].

The mass transfer of species between the bulk solution and the metal surface, where the electroactive species are consumed/produced, defines the concentration of species at the metal–solution interface—the reaction site.

The corrosion rate–predictive models developed to date can be best classified depending on the mathematical description of the abovementioned fundamental thermodynamics and kinetic processes underlying the corrosion process. That includes the following:

- *empirical models* employ arbitrary mathematical expressions with no true theoretical underpinning, similar to the so-called Norsok model [13–15] or the model proposed earlier by Dugstad et al. [16]. Because of this major deficiency these models will not be further discussed in this review;
- *semiempirical models* are based on some rudimentary mechanistic considerations, such as the series of models developed by de Waard and collaborators [1,3,17–20];
- *elementary mechanistic models* that use a theoretical approach similar to what was originally introduced by Gray et al. [4,5,21,22]; and
- *comprehensive mechanistic models* similar to that introduced by Nešić et al. [2,23–25], where majority of the processes are described based on the fundamental physiochemical laws.

With the focus on more recent mechanistic models, the following sections cover a brief historical review of the key studies[1] that had a significant impact on mathematical modeling of the CO_2 corrosion. To make it easier to follow, the mathematical models are grouped into three main classes: *semiempirical*, *elementary mechanistic*, and *comprehensive mechanistic*, based on how deeply they are rooted in the theory of the corrosion process. The general idea behind each group of models, in addition to their advantages and drawbacks are discussed. Furthermore, the relevant mathematical relationships describing various physiochemical aspects of CO_2 corrosion—the building blocks used in developing mechanistic models—are compiled and the appropriate solution method for each group is briefly discussed.

34.2 Water chemistry calculations

Irrespective of the corrosion modeling approach, one of the primary steps for determining the corrosivity of an aqueous CO_2 solution is the so-called water chemistry calculation, used essentially to obtain the concentration of the chemical species involved in the corrosion process. Although aqueous CO_2 is not a corrosive species itself, its hydrated form (H_2CO_3) is a weak acid, often associated with high corrosivity of CO_2 solutions [2–4,22,26]. The term *weak acid* denotes that carbonic acid only partially dissociates in an aqueous solution (also true for the bicarbonate ion). The chemical

[1] This was not meant to be a comprehensive review in a sense that all the models that appeared in the open literature are described.

equilibria can be used to calculate the concentrations of species in an aqueous CO_2 saturated solution, as listed in Table 34.1.

Carbon dioxide dissolution equilibrium, as shown by Reaction (34.2), can be mathematically expressed through Eq. (34.12):

$$\frac{C_{CO_{2(aq)}}}{P_{CO_{2(g)}}} = K_H \tag{34.12}$$

For a binary H_2O-CO_2 system, carbon dioxide partial pressure is $P_{CO_2} = P_{tot} - P_{ws}$, where P_{ws} is the water saturation pressure calculated from Eq. (34.13) with a_i constants shown in Table 34.3 [27].

$$P_{ws} = 10\left[\frac{2C}{-B + (B^2 - 4AC)^{0.5}}\right]^4 \tag{34.13}$$

$$A = \theta^2 + a_1\theta + a_2; \quad B = a_3\theta^2 + a_4\theta + a_5; \quad C = a_6\theta^2 + a_7\theta + a_8;$$

$$\theta = T + \frac{a_9}{T - a_{10}}$$

Assuming a dilute, ideal solution, the equilibrium constant (K_H) can be expressed in terms of modified Henry's constant:

$$K_H = \frac{10^{-3}\rho_w}{(1 + K_{hyd})} e^{\left(-\ln\left(K_H^0\right) - PF + \ln\left(\varphi_{CO_2}\right)\right)} \tag{34.14}$$

where K_H is corrected for unit conversion from molality to molarity with water density ρ_w (see Table 34.4). The term $(1 + K_{hyd})$ is a correction factor that may be relevant, because in majority of CO_2 solubility studies [32,33], the measured concentration of CO_2^* is in fact the sum of concentrations of CO_2 and H_2CO_3. Then the equilibria are discussed in term of Reactions (34.15) and (34.16) with $[CO_2^*] = [CO_2] + [H_2CO_3]$, where carbonic acid is not explicitly considered.

$$CO_{2(g)} \rightleftharpoons CO^*_{2(aq)} \tag{34.15}$$

$$CO^*_{2(aq)} + H_2O_{(l)} \rightleftharpoons HCO^-_{3(aq)} + H^+_{(aq)} \tag{34.16}$$

Therefore, the equilibrium constant of Reaction (34.15) is $K_H{}^* = K_H \times (1 + K_{hyd})$.

The $K_H{}^0$ term in Eq. (34.14) is the Henry's constant of CO_2 dissolution at water saturation pressure shown via Eq. (34.17), where a_i are the constants as shown in Table 34.3 [28]:

$$\ln\left(K_H^0\right) = a_1 + a_2T + \frac{a_3}{T} + \frac{a_4}{T^2} \tag{34.17}$$

Table 34.3 a_i constants of Eqs. (34.13), (34.17), (34.19), (34.22), (34.24), (34.26)[a]

	K_H [28]	φ_{CO_2} [29]	K_{ca} [30]	K_{bi} [30]	K_w [31]	P_{ws} [27]
a_1	1.3000 $E1$	1.0000	233.51593	−151.1815	−4.098	0.1167 $E4$
a_2	−1.3341 $E-2$	4.7587 $E-3$	–	−0.0887	−3245.2	−0.7242 $E6$
a_3	−5.5898 $E2$	−3.3570 $E-6$	−11974.3835	−1362.2591	2.2362	−0.1707 $E2$
a_4	−4.2258 $E5$	–	–	–	−3.984 $E7$	0.1202 $E5$
a_5	–	−1.3179	−36.5063	27.7980	13.957	−0.3233 $E7$
a_6	–	−3.8389 $E-6$	−450.8005	−29.5145	−1262.3	0.1492 $E2$
a_7	–	–	21313.1885	1389.0154	8.5641 $E5$	−0.4823 $E4$
a_8	–	2.2815 $E-3$	67.1427	4.4196	–	0.4051 $E6$
a_9	–	–	0.0084	0.0032	–	−0.2386
a_{10}	–	–	−0.4015	−0.1644	–	0.6502 $E3$
a_{11}	–	–	−0.0012	−0.0005	–	–

[a]The a_i values are rounded to four digits after the decimal.

Table 34.4 Temperature dependence of the physiochemical properties

Parameter	Relationship	References
Water density (kg/m^3)	$\rho_w = 753.596 + 1.87748\ T - 0.003562\ T^2$	[2]
Water viscosity (cP)	$\mu = \mu_{ref} 10^{\left(\frac{1.1709\ (T_{ref}-T)-0.001827(T_{ref}-T)^2}{(T-273.15)+89.93}\right)}$ $T_{ref} = 293.15\ K,\ \mu_{ref} = 1.002\ cP$	[34]
Diffusion coefficient[a]	$D_i = D_{i,ref} \frac{T}{T_{ref}} \frac{\mu_{ref}}{\mu}$	
Molar volume of $CO_{2(aq)}$ (cm^3/mol)	$\widetilde{V_m} = 37.51 - 9.585 \times 10^{-2}\ (T - 273.15) + 8.74 \times 10^{-4}(T - 273.15)^2 - 5.044 \times 10^{-7}(T - 273.15)^3$	[35]
Saturation pressure of CO_2 (mm Hg)	$\log(P_{CO_2 S}) = 7.58828 - \frac{861.82}{(T - 273.15) + 271.883}$	[36]

[a]Reference values are listed in Table 34.7.

The *PF* term in Eq. (34.14) is the so-called Poynting correction factor (Eq. 34.18), which accounts for the change in solution volume as a result of CO_2 dissolution, where $\widetilde{V_m}$ is the partial molar volume of $CO_{2(aq)}$ (see Table 34.4), and P_{ws} is the water saturation pressure calculated via Eq. (34.13).

$$PF = \frac{\widetilde{V_m}(P - P_{ws})}{RT} \tag{34.18}$$

The fugacity coefficient of $CO_{2(g)}$, φ_{CO_2} may be calculated based on the empirical expression of Duan et al. [29], which was shown to agree well with the more complex iterative calculations of the fifth-order virial equation of state used in their earlier study [37].

$$\varphi_{CO_2} = a_1 + \left[a_2 + a_3 T + \frac{a_4}{T} + \frac{a_5}{T - 150}\right]P + \left[a_6 + a_7 T + \frac{a_8}{T}\right]P^2 \tag{34.19}$$

Eq. (34.19) is valid for pressures up to CO_2 saturation pressure (P_{CO_2S} in Table 34.4) when $T < 305$ and at $305 < T < 405$ up to $P = 75 + (T - 305) \times 1.25$, where T and P are in Kelvin and bar, respectively. The K_H values calculated based on Eq. (34.14) were found to be in a good agreement with those of Oddo and Tomson [38] and Weiss [39].

Carbon dioxide hydration equilibrium for Reaction (34.3) may be described by Eq. (34.20).

$$\frac{C_{H_2CO_{3(aq)}}}{C_{CO_{2(aq)}}} = K_{hyd} \tag{34.20}$$

The CO_2 hydration reaction and its equilibrium constant, K_{hyd}, have been discussed by a number of authors [33,40–43]. Although the reported values are not always in good agreement, the lack of temperature dependence of the equilibrium constant has been agreed upon [33,42]. In a more recent study Soli and Byrne [42] reviewed the existing literature briefly and reported $K_{hyd} = 1.18 \times 10^{-3}$ based on their own measurements.

Carbonic acid dissociation, Reaction (34.4), equilibrium is described mathematically through Eq. (34.21):

$$\frac{C_{HCO_{3(aq)}^-} C_{H_{(aq)}^+}}{C_{H_2CO_{3(aq)}}} = K_{ca} \tag{34.21}$$

The temperature–pressure dependence relationship describing K_{ca} have been developed by Li and Duan [28,30] in the form of Eq. (34.22), where the preexponential

terms are the corrections for the units and accounting for the hydration reaction, and a_1–a_{11} are constants as listed in Table 34.3.

$$K_{ca} = \left(1 + \frac{1}{K_{hyd}}\right) 10^{-3} \times \rho_w e^{\left(a1 + a2T + \frac{a3}{T} + \frac{a4}{T^2} + a5\,\ln(T) + \left(\frac{a6}{T} + \frac{a7}{T^2} + \frac{a8}{T}\ln T\right)(p - p_s) + \left(\frac{a9}{T} + \frac{a10}{T^2} + \frac{a11}{T}\ln T\right)(p - p_s)^2\right)} \tag{34.22}$$

The term P_s in Eq. (34.22) is equal to unity at $T < 373.15$ and $P_s = P_{ws}$ at higher temperatures.

Bicarbonate dissociation equilibrium, Reaction (34.5), is mathematically expressed through Eq. (34.23):

$$\frac{C_{CO^{2-}_{3(aq)}} C_{H^+_{(aq)}}}{C_{HCO^-_{3(aq)}}} = K_{bi} \tag{34.23}$$

Li and Duan [28,30] also developed a temperature–pressure dependence relationship for K_{bi}, where P_s and the preexponent terms have a similar meaning to that discussed for carbonic acid dissociation reaction, and a_1–a_{11} values are listed in Table 34.3.

$$K_{bi} = 10^{-3} \rho_w e^{\left(a1 + a2T + \frac{a3}{T} + \frac{a4}{T^2} + a5\,\ln(T) + \left(\frac{a6}{T} + \frac{a7}{T^2} + \frac{a8}{T}\ln T\right)(p - p_s) + \left(\frac{a9}{T} + \frac{a10}{T^2} + \frac{a11}{T}\ln T\right)(p - p_s)^2\right)} \tag{34.24}$$

Water dissociation reaction, shown via Reaction (34.6), is mathematically described by Eq. (34.25):

$$K_w = C_{OH^-_{(aq)}} C_{H^+_{(aq)}} \tag{34.25}$$

The values for K_w can be obtained from the formulation introduced by Marshall and Frank [31] following the form of Eq. (34.26) with a_1–a_7 coefficients listed in Table 34.3. The first term in Eq. (34.26) is also the correction for units conversion from molality to molar concentrations.

$$K_w = \left(10^{-3}\rho_w\right)^2 10^{-\left(a1 + \frac{a2}{T} + \frac{a3}{T^2} + \frac{a4}{T^3} + \left(a5 + \frac{a6}{T} + \frac{a7}{T^2}\right)\log(10^{-3}\rho_w)\right)} \tag{34.26}$$

The equilibrium concentrations of the different chemical species in the bulk solution can be obtained by solving the set of mathematical expressions presented above. In a

solution without an externally induced electric field, the concentration of ions must also satisfy the electroneutrality constraint as shown by Eq. (34.27).

$$\sum_i z_i C_i = 0 \tag{34.27}$$

Assuming an "open" system with an excess of CO_2 gas (i.e., constant $P_{CO_{2(g)}}$), the carbonic acid concentration is defined solely by the $P_{CO_{2(g)}}$, whereas the concentration of the other carbonate species is a function of the solution pH. These can be obtained by considering the electroneutrality equation along with CO_2 chemical equilibria, forming a set of six nonlinear, coupled algebraic equations. These can be solved using various methods (e.g., numerical Newton−Raphson method), to obtain the concentration of the six chemical species: $CO_{2(aq)}$, $H^+_{(aq)}$, $H_2CO_{3(aq)}$, $HCO^-_{3(aq)}$, $CO^{2-}_{3(aq)}$, and $OH^-_{(aq)}$.

The examples of such calculations are demonstrated in Fig. 34.1 through 34.3. Fig. 34.1 shows the comparison of molar fraction of the dissolved CO_2 at various CO_2 partial pressures obtained experimentally [44], with the water chemistry calculations as described earlier. The significant effect of nonideal behavior of CO_2 gas at high partial pressures on the water chemistry can be seen when comparing the calculations based on Henry's law (Eq. 34.17) and the one based on CO_2 fugacity (Eq. 34.19). These results suggest that at partial pressures above 10 bar (145 psi), a significant deviation from ideal conditions should be expected.

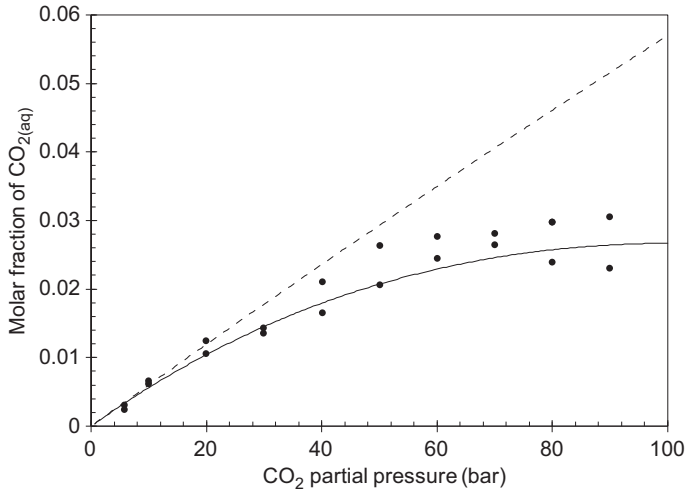

Figure 34.1 Comparison of the experimental molar fraction of dissolved CO_2 in water (*closed circles*) with calculated results based on Henry's law (*dashed line*) and nonideal gas calculations (*solid line*) at 298.15K, as a function of CO_2 partial pressure.
Experimental data taken from M.F. Mohamed, A.M. Nor, M.F. Suhor, M. Singer, Y.S. Choi, Water chemistry for corrosion prediction in high pressure CO_2 environments, in: CORROSION, 2011. Paper No. 375.

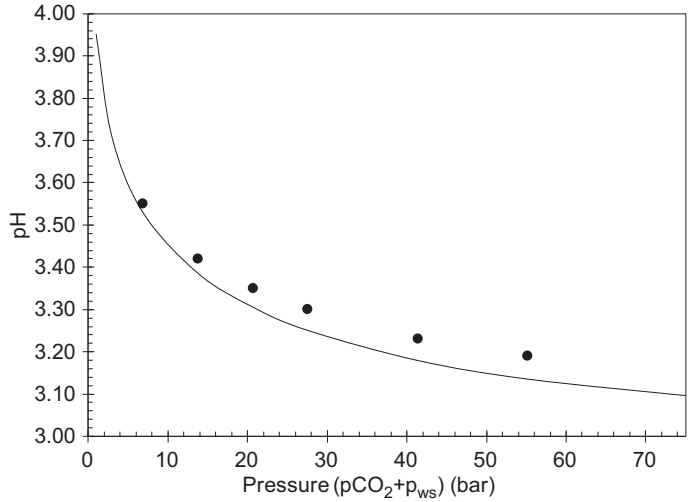

Figure 34.2 Calculated pH of water saturated with $CO_{2(g)}$ at 305.15K, as a function of total pressure (*solid line*) compared with experimental data (*closed circles*), taken from B. Meyssami, M.O. Balaban, A.A. Teixeira, Prediction of pH in model systems pressurized with carbon dioxide, Biotechnology Progress 8 (1992) 149−154, http://dx.doi.org/10.1021/bp00014a009.

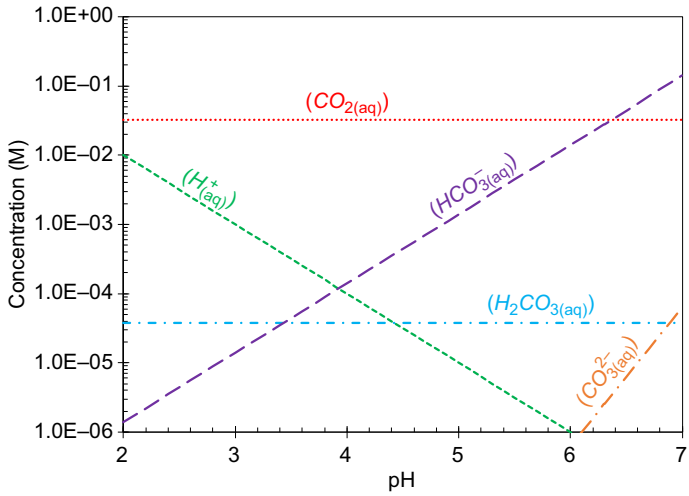

Figure 34.3 Concentration of different species in CO_2/water equilibrium at various acidic pH values and $T = 298.15$K in an open system with a 1 bar total pressure ($P_{CO_2} \simeq 0.968$ bar(14 psi)).

Fig. 34.2 shows the pH of the CO_2 saturated aqueous solutions, obtained at pressures up to 75 bar (1087 psi). These results were in good agreement with the experimental data of Meysammi et al. [45], whereas at higher pressures, some deviations were observed because of the departure from ideal solution assumption.

Similar calculations can be used to determine the chemical composition of an aqueous CO_2 saturated solution. Fig. 34.3 shows the concentration of the species involved in CO_2 equilibria under atmospheric pressure at various pH values.

However, the earlier discussion applies for a particular case where the chemical speciation is only a result of CO_2 equilibria (which is true in condensed water systems, for example). That is not always the case in industrial applications, where additional species and reactions may be present, such as those in formation water. Nevertheless, one can readily introduce the additional species, include additional equilibrium relationships as appropriate, and may perform a very similar calculation then to obtain the speciation for a more complex scenario. That may include the species such as neutral salts (e.g., sodium chloride and calcium chloride, barium sulfate), additional cations, organic acids, hydrogen sulfide, etc.

34.3 The CO_2 corrosion rate calculation

The existing mechanistic mathematical models used for calculating CO_2 corrosion rate can be classified in one of the following groups, when considering their modeling approach and the depth of mechanistic treatment of the involved physiochemical processes [9]:

- *Semiempirical models* are simple tools used to represent the experimentally obtained corrosion rate data. These models are obtained by fitting mathematical functions to a corrosion rate data set. In some cases, these functions may carry some rudimentary mechanistic meanings. These types of models are merely a mathematical reflection of a given experimental data set used to calibrate them and are restricted in validity to the experimental conditions associated with those of the data sets. That makes any extrapolated calculation dubious at best, whereas the expansion to include a wider range of influential variables may require extensive experimentation and a complete reconstruction of the model.
- *Elementary mechanistic models* are developed using the basic understanding of the electrochemical nature of the corrosion process as the basis of the calculations. The current/potential relationships are used to obtain the rate of the surface electrochemical reactions. Using a mechanistic approach, other significant processes such as mass transfer and homogenous chemical reactions may also be incorporated into the corrosion rate calculation. The mathematical relationships used to develop these models are theoretical expressions rooted in fundamental physiochemical theories. That makes these types of models more dependable for corrosion rate prediction across a broader range of environmental conditions (e.g., temperature, flow, pCO_2, pH, etc.), as well as for extrapolation. However, these types of models do resort to certain simplifications to make them easier to understand and resolve mathematically. For example, in these models each electroactive species is treated individually when it comes to mass transfer, and their possible interaction with other species through chemical reactions or electrostatic forces is disregarded.
- *Comprehensive mechanistic models* are based on a detailed description of the solution composition and reactions at the metal−solution interface, expressed through fundamental physiochemical laws. Most of the shortcomings of the elementary mechanistic models are here rectified; for example, they properly incorporate the effect of homogeneous chemical reactions into surface concentration and corrosion rate calculations, while maintaining the accurate mass and charge transfer balances. The comprehensive mathematical models enable

more accurate predictions, they are easier to extend by adding new physics, and their extrapolation capability is limited only by the validity range of the underlying fundamental physicochemical laws and not by the data used to calibrate them. However, to develop these models, a more in-depth mechanistic understanding of the various processes in CO_2 corrosion is required, these models are also more mathematically complex and more computationally demanding.

34.3.1 Semiempirical models

Generally, the semiempirical models are simple predictive tools justifiable when limited fundamental understanding is available. The basic mathematical functions used in these models may originate from rudimentary approximations of the fundamental physicochemical processes underlying the corrosion phenomena; however, the more elaborate aspects are accounted for by introducing correction factors in the model [46,47]. In most cases, these factors are best-fit functions based on limited experimental data with no theoretical significance. This lack of theoretical basis makes any combination of these empirical correction factors (required to cover more complex conditions)—dubious, to say the least. More importantly, these models cannot reliably be extrapolated outside the conditions used for their development. For the same reason these models have little flexibility needed for further extensions to account for new phenomena or new data and require recalibration of the model with the entire data set to accommodate any such extension. To date, many variations of empirical/semiempirical models that address a particular application are found [1,14,16–19,48,49].

In an attempt to focus this review on the more recent mechanistic developments in CO_2 corrosion modeling, the discussion of semiempirical models is limited to a brief review of the work by de Waard et al. because of its significance in shaping the understanding of CO_2 corrosion as we know it today. However, numerous reviews on empirical and semiempirical models are available in the literature for further reference [13,46,47,50–53].

The initial study by de Waard and Milliams in 1975 has been considered the first mechanistic attempt to describe and further, predict the CO_2 corrosion of steel [3]. Using a model developed based on simplistic charge transfer relationships, the authors proposed a catalytic mechanism for CO_2 corrosion as shown via Reactions (34.28) and (34.29). This mechanism considered carbonic acid as the dominant reduced species, whereas its concentration was buffered by the chemical equilibrium between the reaction product $\left(HCO_3^-\right)$ and hydrogen ions present in an acid solution:

$$H_2CO_{3(aq)} + e^- \rightarrow HCO_{3(aq)}^- + \frac{1}{2}H_{2(g)} \tag{34.28}$$

$$HCO_{3(aq)}^- + H_{(aq)}^+ \leftrightharpoons H_2CO_{3(aq)} \tag{34.29}$$

De Waard and Milliams proposed the following relationship for corrosion rate estimation by considering the charge balance at corrosion potential ($i_a = i_c$) and using pH dependence expressions to relate the potential to corrosion current [3]:

$$\log i_{corr} = -A\ \mathrm{pH} + B \tag{34.30}$$

The term A in Eq. (34.30) is only defined by the Tafel slopes of the cathodic and anodic reactions, whereas the term B also contains the reaction rate constants. The correlation coefficient in Eq. (34.30), A, was experimentally obtained to be 1.3. This value was used as the basis for their proposed mechanism, which gives the theoretical value of 1.25, considering 40 and 120 mV Tafel slopes for anodic and cathodic reactions, respectively. Ultimately, using a simplistic correlation between the solution pH and CO_2 partial pressure, de Waard and Milliams introduced their well-known nomogram for corrosion rate calculation as a function of CO_2 partial pressure, based on the following relationship [1]:

$$\log i_{corr} = -1/2\, A \log(pCO_2) + B' \tag{34.31}$$

The initial model developed by de Waard and Milliams did not include the effect of other electroactive species, such as hydrogen ion, bicarbonate ion, and water; the pH was assumed to only be defined by the CO_2 equilibria; and the effect of mass transfer, CO_2 hydration reaction, and other homogeneous chemical reactions associated with carbonate species was also disregarded [3]. That made the model simple but narrowed the range of its applications drastically.

In a series of studies, extending over almost two decades, the initial model of de Waard and Milliams [3] was used as the basis to add in the effect of various relevant parameters and environmental conditions [1,17–20]. The effect of pH, flow rate, nonideal solutions, protective scales, glycol, top of line corrosion, and steel microstructure are among those covered in the subsequent publications of de Waard et al. [1,17–20]. These new effects were accounted for by simply introducing additional empirical correction factors as multipliers in the original de Waard and Milliams correlation. That transformed the original mechanistic approach of de Waard and Milliams into a semiempirical model with all the disadvantages discussed earlier.

34.3.2 Elementary mechanistic models

In the context of aqueous CO_2 corrosion of steel, the deterioration is due to the electrochemical oxidation of iron as shown in Reaction (34.7), which results in dissolution of iron and release of electrons. This reaction would spontaneously progress only if the released electrons are consumed through simultaneous cathodic reactions (Reactions 34.8–34.11). The corrosion rate is therefore defined by the charge balance between cathodic and anodic reactions at the steel surface. Hence, it can be mathematically expressed by describing the current/potential response of the underlying electrochemical reactions. Based on this scenario, the corrosion rate is equal to the iron oxidation (dissolution) rate when

$$i_a = \sum_j i_{c,j}$$

As outlined in Section 34.3.1, the same expression served as the basis for the first model of de Waard and Milliams [3]; however, they only considered reduction of

carbonic acid as the main cathodic reaction and rate-controlling step. The elementary mechanistic models expanded on this to include the other relevant physiochemical processes such as additional cathodic reactions, mass transfer, and chemical reactions, in the calculation of the charge transfer rates. This gave these models a much improved ability to incorporate the more advanced understanding of CO_2 corrosion, without making them overly complicated.

34.3.2.1 Historical background

The first elementary mechanistic model for CO_2 corrosion of steel was introduced in 1989 by Gray et al. [4]. The authors developed their model with iron dissolution as the anodic reaction and hydrogen ion and carbonic acid reduction as the cathodic reactions. Their model accounted for the mass transfer at a rotating disk electrode for hydrogen ion and carbonic acid reduction. The effect of CO_2 hydration reaction was also incorporated in the charge transfer calculation of carbonic acid reduction. Gray et al. [4] adopted most of the mechanistic findings of Schmitt and Rothmann [26], while suggesting that the preceding adsorption step for CO_2 hydration reaction was unnecessary in predicting the observed polarization behavior.

Gray and coworkers expanded their experimental conditions toward higher pH values in a later publication, covering up to pH 10 [5]. The authors suggested that at a pH range of 6−10 the reduction of bicarbonate ion becomes significant, and the original model was expanded to also include the bicarbonate ion reduction. The mechanism for CO_2 corrosion of steel, as proposed by Gray et al. in these two studies [4,5], has rapidly gained general acceptance and was further developed in the following years.

In 1995 Dayalan et al. proposed a model based on equating the mass transfer and charge transfer of electroactive species at the metal surface and imposing the chemical equilibria of the carbonic acid and bicarbonate ion dissociation [54]. This set of algebraic equations was then solved to obtain the surface concentration of chemical species as well as the corrosion potential. This was an ambitious step forward, yet the model proposed by Dalayan et al. suffered from miscalculations in charge transfer rates, did not include the temperature effect, and did not account for the effect of CO_2 hydration reaction. Even with these shortcomings, this model was of significance because it provided the first insight into the surface concentration of species, which are necessary for protective iron carbonate layer formation calculations [55]. Furthermore, this study was one of the first to discuss and incorporate carbonic acid and bicarbonate ion dissociation reactions at the metal surface.

In 1996, an elementary mechanistic model was also developed by Nešić et al., mainly focused on improving the estimated electrochemical rate constants and implementation of this mechanistic approach into corrosion rate prediction for industrial applications [22]. This model was developed by considering the mass transfer, CO_2 hydration reaction, and the kinetics of the electrochemical reactions similar to that previously proposed by Gray et al. [4,5]. Hydrogen ion, carbonic acid, water, and oxygen reduction was included in the model as the possible cathodic reactions and iron dissolution as the only anodic reaction. In this model, Nešić et al. assumed that the carbonic acid reduction was only limited by the CO_2 hydration reaction, as the preceding chemical reaction step, and the

effect of mass transfer on the chemical reaction limiting current of carbonic acid reduction was ignored. Although such an assumption is reasonable for stagnant conditions, it may lead to significant errors at high solution velocities where the rate of mass transfer is comparable with the rate of the chemical reaction. This issue was addressed by Nešić et al. in a later publication where the effect of mass transfer was also included in chemical reaction limiting current calculations for turbulent flow regimes [21].

The elementary mechanistic models are now well established for calculation of internal pipeline corrosion rates. After the initial study by Gray et al. [4,5], numerous similar models have been developed and used to improve the mechanistic understanding of the corrosion process as well as the accuracy of the predicted corrosion rates [56–61]. The scope of these models was expanded to incorporate more complex scenarios such as the effect of corrosion product layer [55,62], multiphase flow [63], and the presence of other corrosive species such as oxygen, hydrogen sulfide, and organic acids [11,21,57,61,64,65].

34.3.2.2 Mathematical description

The net current density resulting from the electrochemical reactions occurring at the metal surface can be obtained by superposition of the current density from every individual reaction (i_j) as shown in Eq. (34.32).

$$i_{net} = \sum_j i_j \tag{34.32}$$

For the electrochemical reactions involved in aqueous CO_2 corrosion of steel, the current/potential relationships are given in Table 34.5. Considering the heterogeneity of the electrochemical reactions, the concentration terms appearing in these relationships represent the concentration at the metal surface, which may be different from the bulk concentrations as a result of the mass transfer limitation. Nevertheless, the effect of mass transfer on the surface concentration of electroactive species and thus the rate of electrochemical reactions can be incorporated in current density calculations through Eq. (34.33).

$$\frac{1}{i} = \frac{1}{i_{ct}} + \frac{1}{i_{lim}} \tag{34.33}$$

The term i_{ct} in Eq. (34.33) is the pure charge transfer controlled current, which is obtained from the relationships listed in Table 34.5, where the surface concentrations of electroactive species are equal to bulk concentrations at the pure charge transfer control condition. The electrochemical parameters required for charge transfer calculations are listed in Table 34.6. The i_{lim} term in Eq. (34.33) is the mass transfer limiting current as described in Eq. (34.34).

$$i_{lim} = nFk_m C^b \tag{34.34}$$

Table 34.5 Current potential relationships for the reactions listed in Table 34.2

Electrochemical reaction	Mathematical relationship for half reaction[a]
Reaction (34.7)	$i_{a,\mathrm{Fe}} = n_{\mathrm{Fe}} F k_{0_{\mathrm{Fe}}} C^{s}_{\mathrm{OH}^-} e^{\left(\frac{(2-\alpha_{\mathrm{Fe}})F\left(E_{app}-E_{0_{\mathrm{Fe}}}-\phi_s\right)}{RT}\right)}$[b]
Reaction (34.8)	$i_{c,\mathrm{H}^+} = -n_{\mathrm{H}^+} F k_{0_{\mathrm{H}^+}} C^{s}_{\mathrm{H}^+} e^{\left(\frac{-\alpha_{\mathrm{H}^+} n_{\mathrm{H}^+} F\left(E_{app}-E_{0_{\mathrm{H}^+}}-\phi_s\right)}{RT}\right)}$
Reaction (34.9)	$i_{c,\mathrm{H_2O}} = -n_{\mathrm{H_2O}} F k_{0_{\mathrm{H_2O}}} e^{\left(\frac{-\alpha_{\mathrm{H_2O}} n_{\mathrm{H_2O}} F\left(E_{app}-E_{0_{\mathrm{H_2O}}}-\phi_s\right)}{RT}\right)}$
Reaction (34.10)	$i_{c,\mathrm{H_2CO_3}} = -n_{\mathrm{H_2CO_3}} F k_{0_{\mathrm{H_2CO_3}}} C^{s}_{\mathrm{H_2CO_3}} e^{\left(\frac{-\alpha_{\mathrm{H_2CO_3}} n_{\mathrm{H_2CO_3}} F\left(E_{app}-E_{0_{\mathrm{H_2CO_3}}}-\phi_s\right)}{RT}\right)}$
Reaction (34.11)	$i_{c,\mathrm{HCO_3^-}} = -n_{\mathrm{HCO_3^-}} F k_{\mathrm{HCO_3^-}} C^{s}_{\mathrm{HCO_3^-}} e^{\left(\frac{-\alpha_{\mathrm{HCO_3^-}} n_{\mathrm{HCO_3^-}} F\left(E_{app}-E_{0_{\mathrm{HCO_3^-}}}-\phi_s\right)}{RT}\right)}$

[a] i_c and i_a denote the current density calculations for cathodic half reactions and anodic half reactions, respectively.
[b] ϕ_s is the potential in the solution at adjacent to the metal surface, which accounts for ohmic drop if applicable.

Table 34.6 Electrochemical parameters for the relationships in Table 34.5, where $k_{0_j} = k_{0_{j,ref}} e^{\left(-\frac{\Delta H_j}{R}\left(\frac{1}{T} - \frac{1}{T_{j,\,ref}}\right)\right)}$

	n_j	α_j	$E_{0,j}$ versus SHE (V)	$k_{0\ j,\ ref}$	ΔH_j (kJ/mol)	$T_{j,\ ref}$ (K)
$j = \mathrm{Fe}$	2	0.5^a	-0.447^b	$1.59 \times 10^5 \left(\frac{\mathrm{mol}}{\mathrm{s \cdot m^2 \cdot M}}\right)^a$	37.5^a	298.15^a
$j = \mathrm{H^+}$	1	0.5^a	0.000	$5.18 \times 10^{-5} \left(\frac{\mathrm{mol}}{\mathrm{s \cdot m^2 \cdot M}}\right)^a$	30^a	298.15^a
$j = \mathrm{H_2O}$	1	0.5^c	-0.8277^b	$2.70 \times 10^{-5} \left(\frac{\mathrm{mol}}{\mathrm{s \cdot m^2}}\right)^c$	30^c	293.15^c
$j = \mathrm{H_2CO_3}$	1	0.5^a	-0.381^f	$3.71 \times 10^{-2} \left(\frac{\mathrm{mol}}{\mathrm{s \cdot m^2 \cdot M}}\right)^a$	50^a	293.15^a
$j = \mathrm{HCO_3^-}$	1	0.5^d	-0.615^f	$7.37 \times 10^{-5} \left(\frac{\mathrm{mol}}{\mathrm{s \cdot m^2 \cdot M}}\right)^d$	50^e	298.15^e

Parameters obtained or recalculated from, *a*: Nordsveen et al. [2], *b*: CRC Handbook [73], *c*: Zheng et al. [11], *d*: Gray et al. [5], *e*: Han et al. [57], *f*: Linter and Burstein [74].

The mass transfer coefficients (k_m) for variety of common flow geometries are readily available in the literature. For example, the well-known Levich equation is used to calculate the mass transfer limiting current density at a rotating disk electrode as shown in Eq. (34.35) [8]:

$$i_{lim} = 0.62 \times 10^3 \, nFD^{2/3}\omega^{1/2}\nu^{-1/6}C_b \tag{34.35}$$

where C_b is the bulk molar concentration of the reactant, ω (rad/s) is angular velocity, D is the diffusion coefficient as listed in Table 34.7 for the common chemical species, and other parameters are in SI units.

For a rotating cylinder electrode, a correlation developed by Eisenberg et al. [66] (simplified as Eq. 34.36) or similar expressions [67] may be used. In Eq. (34.36) the bulk concentration of the active species, C_b, is in molar, d_{cyl} is the diameter of the cylinder electrode in meter, and other parameters have their common meaning in SI units.

$$i_{lim} = 0.0487 \times 10^3 \, nFD^{0.644}d_{cyl}^{0.4}\omega^{0.7}\nu^{-0.344}C_b \tag{34.36}$$

The mass transfer correlation in fully developed single-phase turbulent flow through straight pipes was developed by Berger and Hau [67a], where the Sherwood number (Sh) is correlated to the Reynolds number (Re) and the Schmidt number (Sc), as shown in Eq. (34.37), and the mass transfer coefficient can be obtained using $k_m = Sh \cdot D/L$.

$$Sh = 0.0165 \, Re^{0.86}Sc^{0.33} \tag{34.37}$$

$$8 \times 10^3 < Re < 2 \times 10^5, \quad 1000 < Sc < 6000$$

Table 34.7 Reference diffusion coefficients at 25°C (77°F)

Species	Diffusion coefficient in water $\times 10^9$ (m^2/s)	References
CO_2	1.92	[94]
H_2CO_3	2.00	[2]
HCO_3^-	1.185	[73]
CO_3^{2-}	0.923	[73]
H^+	9.312	[85]
OH^-	5.273	[73]
Na^+	1.334	[85]
Cl^-	2.032	[73,85]
Fe^{2+}	0.72	[85]

For many other flow regimes and geometries such as multiphase flow, U-bends, and elbows, similar correlations also exist in the literature [68–72].

In addition to the mass transfer from the bulk solution, the effect of slow CO_2 hydration reaction on the carbonic acid reduction needs to be included in calculations. In this case also, Eq. (34.33) can be used whereas the mass transfer limiting current (i_{lim}) has to be modified for simultaneous accommodation of the preceding chemical reaction through the diffusion layer. At a rotating disk electrode, the limiting current density for an electrochemical Reaction (34.39) proceeding a generic homogeneous Reaction (34.38) can be calculated via Eq. (34.40) [75]. These equations can be readily applied for the case of CO_2 corrosion with the chemical reaction being CO_2 hydration and the electrochemical reaction being carbonic acid reduction, as implemented in the models developed by Gray et al. [4,5].

$$\mathrm{Y} \rightleftharpoons \mathrm{O} \tag{34.38}$$

$$\mathrm{O} + ne^- \rightleftharpoons R \tag{34.39}$$

$$i_{lim,\mathrm{O}} = \frac{nFD\left(C_{\mathrm{O}}^b + C_{\mathrm{Y}}^b\right)}{\delta_d + \delta_r/K} \tag{34.40}$$

$$\delta_d = 1.61\, D^{1/3}\omega^{-1/2}\upsilon^{1/6} \tag{34.41}$$

$$\delta_r = \left(\frac{D}{(k_f + k_b)}\right)^{1/2} \tag{34.42}$$

The δ_d term in Eq. (34.40) is the diffusion layer thickness that can be calculated via Eq. (34.41), and δ_r is the so-called reaction layer thickness as described via Eq. (34.42).

Nešić et al. proposed a similar relationship for turbulent flow conditions such as the cases of rotating cylinder electrodes or pipeline flow, using a series of assumption suitable for the particular case of CO_2 corrosion [76]. Based on their proposed relationship, the limiting current for carbonic acid reduction can be calculated as shown in Eq. (34.43), considering both turbulent mixing and the slow hydration of CO_2.

$$i_{lim,\mathrm{H_2CO_3}} = n_{\mathrm{H_2CO_3}} F C_{\mathrm{H_2CO_3}}^b \left(D\, k_{b,hyd}\right)^{1/2} \coth\frac{\delta_d}{\delta_r} \tag{34.43}$$

$$\delta_d = D/k_m \tag{34.44}$$

$$\delta_r = \left(D/k_{b,hyd}\right)^{1/2} \tag{34.45}$$

Table 34.8 List of equations required to describe the current/potential response of each electroactive species

Reaction	Corresponding mathematical relationships
Iron oxidation	Eq. (34.7)
Hydrogen ion reduction	Eqs. (34.8), (34.33), (34.34)
Carbonic acid reduction	Eqs. (34.10), (34.33), (34.40) or Eq. (34.43)
Bicarbonate ion reduction	Eqs. (34.11), (34.33), (34.34)
Water reduction	Eq. (34.9)

Based on the discussions in this section so far, the current/potential response of the commonly accepted electrochemical reactions involved in CO_2 corrosion can be calculated. The relevant relationships to calculate the rate of each reaction are summarized in Table 34.8. For iron oxidation or water reduction reactions, no mass transfer consideration is required because of the constant concentration of the reactant, thus, the current density resulting from these reactions can be calculated via Eqs. (34.7) and (34.9) (in Table 34.5), respectively. For hydrogen ion, carbonic acid, and bicarbonate ion reduction, Eq. (34.33) should be used to account for the mass transfer and chemical reactions as required.

Using the mathematical relationships as summarized in Table 34.7, at a known electrode potential the current density from every individual reaction may be readily obtained. On the other hand, if the electrode potential is unknown, such as in the case of corrosion rate calculations, the current density/potential relationships of all the reactions can be introduced into Eq. (34.32), forming a single nonlinear algebraic equation to be solved for one unknown, the electrode potential. The corrosion potential (mixed potential) can be obtained using numerical root finding methods such as bisection or Newton−Raphson. Finally, the anodic current density calculated via Eq. (34.7) at corrosion potential yields the corrosion current. This value can be further translated to corrosion rate based on Faraday's law and proper unit conversion. For example, for corrosion current i_{corr} (A/m^2) the conversion to corrosion rate (mm/year) is

$$CR = \frac{i_{Corr}}{2F} \times \frac{Mw_{\mathrm{Fe}}}{\rho_{\mathrm{Fe}}} \times 3600 \times 24 \times 365 \tag{34.46}$$

An example of the elementary mechanistic models has been developed and published as an open source code for public users by Nešić et al. [21] called FREECORP. This model is based on the physiochemical processes discussed earlier and can be considered as an improved version of their initial study published in 1996 [22]. The model includes the effect of flow for rotating cylinder electrodes and straight pipelines, the effect of CO_2 hydration reaction, additional corrosive species such as oxygen, acetic acid, and hydrogen sulfide, and the effect of corrosion product layer.

Fig. 34.4 demonstrate a comparison of the predicted steady state voltammogram by the model developed by Nešić et al. with experimental data at pH 4 and 1 bar pCO_2 [21]. The predicted corrosion rates using the same model [21] are also compared with the experimental data in Fig. 34.5 for a wide range of solution composition and environmental conditions.

34.3.2.3 Summary

The development of the elementary mechanistic models created a platform to apply the more recent understandings of the CO_2 corrosion into corrosion rate predictions. With the mechanistic approach in the calculations, these models also provided the opportunity for investigating the individual underlying processes. The elementary mechanistic models are used to quantify the polarization behavior (usually the steady state voltammograms) of the system to obtain the physiochemical parameters involved in various underlying processes, i.e., reaction rate constants of the electrochemical reaction and their activation energies, kinetic, and thermodynamic parameters describing the homogeneous reactions, mass transfer coefficient, etc. The mechanistic nature of the model, and the parameters obtained during the model development, allows for more confident extrapolated corrosion rate calculations. For the same reason, these models have the flexibility to easily include additional corrosive species and, to some extent, new physics.

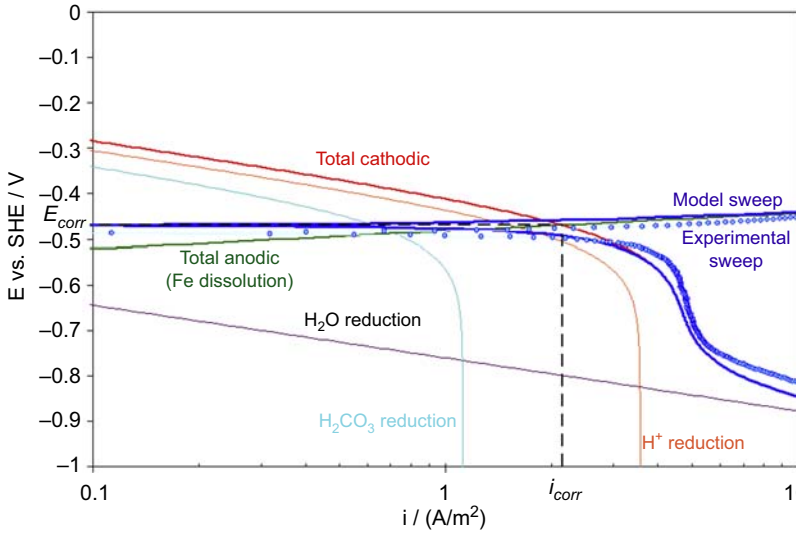

Figure 34.4 Comparison of the predicted steady state polarization behavior (*solid lines*) with the experimental data (*points*) at 20°C (68°F), 1 bar (14.5 psi) CO_2, pH 4, pipe diameter of 0.015 m, and flow velocity of 2 m/s.

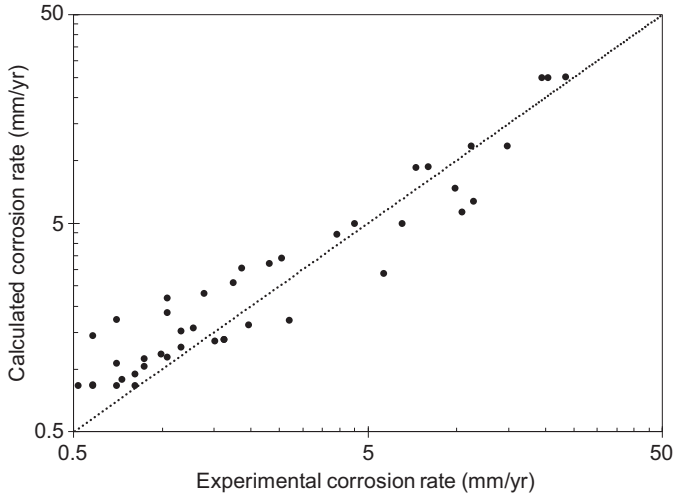

Figure 34.5 Comparison of the experimental and predicted corrosion rates at pCO_2 from 1 to 10 bar (14.5−145 psi), temperature from 20 to 60°C (68−140°F), flow velocity from stagnant to 12 m/s, pH from 4 to 6, and acetic acid concentration from 0 to 390 ppm.
Data taken from S. Nešić, H. Li, J. Huang, D. Sormaz, An open source mechanistic model for CO_2/H_2S corrosion of carbon steel, in: CORROSION, 2009. Paper No. 572.

However, the simple approach of implementation of physicochemical theory in the elementary mechanistic models discussed here suffers from one fundamentally flawed assumption. In these models it is assumed that species are transferred from the bulk fluid toward the metal surface and back independently from each other. In other words, the well-defined homogeneous chemical reactions as well as the ionic interaction (electromigration) between species inside the diffusion layer are ignored.

34.3.3 Comprehensive mechanistic models

The comprehensive mechanistic models are developed based on the fundamental physicochemical laws describing the processes involved in the corrosion phenomena. Using such a rigorous fundamental approach gives these models a great advantage in simulating elaborate, interconnected processes underlying CO_2 corrosion with its complex water chemistry, mass transfer, and electrochemical reactions. For the same reason, these models by nature have a broad range of validity across varying environmental conditions—as long as the used physiochemical laws hold true—and the flexibility to incorporate additional processes and chemical species.

The in-depth treatment of the underlying processes in these models provides a unique insight into the possible reaction pathways and the significance of individual processes, which in turn, further improves the understanding of CO_2 corrosion mechanism. For example, the significance of the buffering ability of weak acids such as carbonic acid and organic acids were not well understood until these models emerged [2,6,77].

The comprehensive mathematical models are built around the mass transfer and homogeneous chemical reactions in the solution near the metal surface; the two key elements in CO_2 corrosion. This can be expressed as the well-known Nernst–Planck equation:

$$\frac{\partial C_i}{\partial t} = -\nabla \cdot N_i + R_i$$

where N_i represents the mass transfer via molecular diffusion, electromigration, convective flow, and turbulent mixing, and the R_i includes the homogeneous chemical reactions. Using the proper boundary conditions along with the Nernst–Planck equation, as discussed in Section 34.3.3.3, the concentration distribution of the chemical species and the rate of electrochemical reactions (hence the corrosion rate) can be accurately determined.

34.3.3.1 Historical background

The first attempt to describe the CO_2 corrosion with the general approach of the comprehensive mathematical models was by Turgoose et al. in 1992 [78]. The mathematical model developed in that study accounted for the mass transfer by diffusion and convective flow as well as homogeneous chemical reactions as independent phenomena in series, rather than the simultaneous treatment as in the Nernst–Planck equation. Despite that deficiency, the authors were able to demonstrate the potential of this type of modeling in providing detailed information about the concentration distribution of chemical species in the diffusion layer. It was shown that the various corrosion mechanisms proposed previously, such as the catalytic mechanism (EC′) proposed by de Waard and Milliams [3] and Więckowski et al. [79] or the CE mechanism proposed by Schmitt and Rothmann [26], are only limited interpretations of a complex water chemistry coupled with electrochemical reactions. However, the authors ignored the charge transfer kinetics of both cathodic and anodic reactions, and the model was only used to calculate the current response at mass transfer limiting condition.

In 1995, Pots developed the first comprehensive mathematical model utilizing the Nernst–Planck equation to simultaneously account for the mass transfer and homogeneous chemical reactions at the solution near the metal surface [77]. The charge transfer rates were assumed to follow the Tafel equation as the boundary conditions at the metal/solution interface. In that study also, the corrosion under mass transfer limiting conditions was at focus and much of the details about the kinetics of the electrochemical reactions were ignored. In such conditions, Pots noted that the carbonic acid reduction at the metal surface is not necessarily required to explain the limiting current, and that its effect may be also explained through the parallel homogeneous carbonic acid dissociation followed by hydrogen ion reduction. That was one of the first reports on the significance of the buffering ability of carbonic acid (or other weak acids [8]) during the corrosion process, which was quantified by employing the comprehensive mathematical models.

The comprehensive mathematical models of CO_2 corrosion of steel were further improved in a series of publications by Nešić et al. [2,23–25,80]. Besides the use of

Nernst–Planck equation to describe the concentration profile of the chemical species in the solution, the homogeneous chemical and electrochemical reactions were treated with more details than in the previous models [77,78]. The scope of the model was further expanded by demonstrating its ability to incorporate the corrosion product layer formation and determining the porosity distribution throughout that layer. The buffering ability of carbonic acid, as reported by Pots [77], was also confirmed by Nešić et al. [2,23]. However, the authors noted that while the carbonic acid reduction reaction was not required to explain the observed limiting currents in polarization curves, this additional cathodic reaction significantly improved the corrosion rate prediction when the corrosion current was controlled by the rate of electrochemical reactions.

In a study by Remita et al., the mechanism of CO_2 corrosion was revisited using a similar modeling approach for quantitative analysis of the experimental data [6]. In that study, authors simplified the model introduced by Nešić et al. [2,23], using steady state calculation (i.e., $dC/dt = 0$ in Nernst–Planck Equation). Using their model, Remita et al. analyzed the experimental cathodic polarization curves and claimed that not only the limiting currents can be fully explained through the buffering effect of carbonic acid but also the charge transfer–controlled currents may be quantified only through the hydrogen ion reduction reaction.

The comprehensive mathematical models, with their analytical approach, have attracted many researchers in the last decades. In more recent years, similar models have been developed and used to describe various corrosion scenarios. A few examples are the studies of sour corrosion by Triobollet et al. [12,81], CO_2 corrosion under a thin water film by Remita et al. [82], pit propagation in CO_2 and acetic acid environment by Amri et al. [83], and top of the line corrosion by Zhang et al. [84].

34.3.3.2 Mathematical description

Since heterogeneous electrochemical reactions are involved in CO_2 corrosion, the concentration of the chemical species at the metal surface may deviate from those at the bulk solution. The comprehensive mathematical models are able to accurately calculate the surface concentration of chemical species based on the known concentrations at the bulk, and with simultaneous consideration of the mass transfer between the bulk and the surface along with the homogeneous chemical reactions.

The mass transfer in corroding systems, or electrochemical systems in general, occurs via three simultaneous mechanisms: *convective flow* due to the (turbulent) movement of the bulk fluid; *molecular diffusion*, as a result of the concentration gradient of the species; *electromigration* of the ions, arising from the presence of an induced or a spontaneous electric field. Hence, the flux of any given species i can be described through Eq. (34.47) [85].

$$N_i = -z_i u_i F C_i \nabla\phi - D_i \nabla C_i + v C_i \tag{34.47}$$

The concentration of each chemical species at an elementary volume of the solution can therefore be defined through its flux and by applying mass conservation. The change in concentration of species i over the time interval of Δt is defined by the

change in its flux over Δx, in addition to the rate of consumption/production of species i through homogeneous chemical reactions. This is mathematically expressed via Eq. (34.48), which is also known as the Nernst–Planck equation [85].

$$\frac{\partial C_i}{\partial t} = -\nabla \cdot N_i + R_i \tag{34.48}$$

For most practical applications, the tangential and radial components of Eqs. (34.47) and (34.48) are not of any practical significance. Furthermore, the mobility of ions can be estimated using Einstein–Smoluchowski relationship ($u_i = D_i/RT$). Therefore, for a one-dimensional semi-infinite geometry in the direction x normal to the metal surface, Eqs. (34.47) and (34.48) can be simplified to Eqs. (34.49) and (34.50), respectively.

$$N_i = -D_i \frac{\partial C_i}{\partial x} - \frac{z_i D_i F C_i}{RT} \frac{\partial \phi}{\partial x} + v_x C_i \tag{34.49}$$

$$\frac{\partial C_i}{\partial t} = -D_i \frac{\partial}{\partial x} \frac{\partial C_i}{\partial x} - \frac{\partial}{\partial x} \left(\frac{z_i D_i F C_i}{RT} \frac{\partial \phi}{\partial x} \right) + v_x \frac{\partial C_i}{\partial x} + R_i \tag{34.50}$$

The average bulk movement of the fluid in the direction normal to the surface is accounted for in the convective flow term ($v_x C$), where v_x describes the velocity profile inside the diffusion layer. Unlike the elementary mechanistic models, where all the mass transfer processes are lumped into a single parameter (mass transfer coefficient, k_m), the comprehensive mathematical models implement the velocity distribution of the fluid inside the diffusion layer. For a laminar flow regime of rotating disk electrodes, the analytical solution of the velocity profile and the diffusion layer thickness were shown as Eq. (34.51), where $a = 0.510$, and Eq. (34.52), respectively [86].

$$v_x = -a\omega \left(\frac{\omega}{\upsilon} \right)^{1/2} x^2 \tag{34.51}$$

$$\delta = \left(\frac{3 D_{lim}}{a v} \right)^{1/3} \left(\frac{\omega}{\upsilon} \right)^{-1/2} \tag{34.52}$$

However, at the conditions of interest for most corrosion applications, the dominant mass transfer mechanism in the bulk solution is in the form of turbulent mixing, which then decays as the solid wall is approached—in the diffusion boundary layer. The turbulent mixing of the fluid can be expressed as eddy diffusivity profile within the diffusion boundary layer. The mathematical relationships for eddy diffusivity of turbulent flow through straight tubes have been developed in a number of different studies [87,88]. A simple expression for eddy diffusivity (D_t) distribution and diffusion layer thickness (δ) is shown in Eqs. (34.53) and (34.54), respectively [88].

$$D_t = 0.18 \left(\frac{x}{\delta} \right)^3 \upsilon \tag{34.53}$$

$$\delta = 25\, Re^{-7/8} d \tag{34.54}$$

The eddy diffusivity (D_t) can be lumped with molecular diffusion coefficient (D_i) in Eqs. (34.49) and (34.50), to account for the turbulent mixing, whereas the convective flow term ($v_x C$) is no longer applicable.

An accurate account of the homogeneous chemical reactions involved in the complex water chemistry of CO_2 saturated solution is essential for calculating the surface concentration of the chemical species. This is of significance, because the buffering system of the solution containing weak acids such as carbonic acid, organic acids, and hydrogen sulfide may act as an additional source (or sink) for the chemical species as their surface concentrations depart from the equilibrium at the bulk solution. The effect of these homogeneous reactions is reflected in the R_i term of Eq. (34.50).

The rate of each chemical reaction j in the general form of Reaction (34.55) can be calculated as shown in Eq. (34.56).

$$\sum_{r=1}^{n_r} C_r \rightleftharpoons \sum_{p=1}^{n_p} C_p \tag{34.55}$$

$$R_j = k_{f,j} \prod_{r=1}^{n_r} C_r - k_{b,j} \prod_{p=1}^{n_p} C_p \tag{34.56}$$

With simple mathematical manipulation, the rate of production (or consumption) of every species i (R_i) for j chemical reactions shown in Table 34.1 may be expressed in a matrix format as Eq. (34.57) [2]. The kinetic rate constant of the chemical reactions can be found in Table 34.9.

$$\begin{bmatrix} R_{CO_{2(aq)}} \\ R_{H^+_{(aq)}} \\ R_{H_2CO_{3(aq)}} \\ R_{HCO^-_{3(aq)}} \\ R_{CO^{2-}_{3(aq)}} \\ R_{OH^-_{(aq)}} \end{bmatrix} = \begin{bmatrix} 1 & -1 & 0 & 0 & 0 \\ 0 & 0 & 1 & 1 & 1 \\ 0 & 1 & -1 & 0 & 0 \\ 0 & 0 & 1 & -1 & 0 \\ 0 & 0 & 0 & 1 & 0 \\ 0 & 0 & 0 & 0 & 1 \end{bmatrix} \times \begin{bmatrix} R_{dis} \\ R_{hyd} \\ R_{ca} \\ R_{bi} \\ R_w \end{bmatrix} \tag{34.57}$$

Considering the discussion so far in this section, Eq. (34.50) can be applied for each chemical species to determine its concentration distribution inside the diffusion layer. The diffusion coefficients of the chemical species and the physical properties of water can be found in Tables 34.7 and 34.4, respectively. However, for this system of equations to be complete, the electric potential appearing in the electromigration term also needs to be specified. This parameter can be characterized through an additional relationship

Table 34.9 Rate constants for reactions listed in Table 34.1 k_f denotes the reaction progress from left to right and $K = k_f/k_b$

Reactions #	Reaction rate constant	References
(34.3)	$k_{f,hyd} = e^{\left(22.66 - \frac{7799}{T}\right)}\ (1/\mathrm{s})$	[42]
(34.4)	$k_{b,ca} = 4.7 \times 10^{10}\ (1/\mathrm{M \cdot s})$	[89–91]
(34.5)	$k_{b,bi} = 5.0 \times 10^{10}\ (1/\mathrm{M \cdot s})$	[89,91][a]
(34.6)	$k_{b,w} = 1.4 \times 10^{11}\ (1/\mathrm{M \cdot s})$	[90,92]

[a]In the absence of direct measurements the value of $k_{b,bi}$ was estimated based on $k_{b,ca}$.

known as the Poisson's equation, which relates the electric potential in a medium with a uniform dielectric constant, to a given charge distribution [85]:

$$\nabla^2\phi = -\frac{F}{\varepsilon}\sum_i z_i C_i \tag{34.58}$$

Although Eq. (34.58) is a more valid theoretical description of the electric potential distribution inside the diffusion layer, a simplified expression known as the "electroneutrality" constraint (Eq. 34.59) has commonly been used as an approximation in mathematical simulation of electrochemical systems:

$$\sum_i z_i C_i = 0 \tag{34.59}$$

This simplification is based on the very large values of the proportionality constant in Poisson's equation (F/ε) [85]. With the relative dielectric constant of saline water being in the range of 60–80 for salt concentrations up to 1 M [93], this proportionality constant would be in order of 10^{14} V·m/C. Therefore, while the electroneutrality constraint is not a fundamental law of nature, it is a reasonable mathematical simplification for the electrochemical systems with moderate or high ionic conductivity where the Laplacian of the potential ($\nabla^2\phi$) is not numerically significant when considering the proportionality constant. In such conditions, the resulting error arising from this assumption is generally well below the error threshold considered for the numerical methods in use. This assumption is favored in mathematical models because it significantly simplifies the mathematical expressions and notably decreases the computational demands of the calculations.

It should be noted that, in mathematical models of electrochemical systems, it is also common to assume that the effect of electromigration on concentration distribution of electroactive species is negligibly small. This allows for the electromigration term appearing in Eq. (34.47) to be disregarded, which simplifies the calculations significantly. Bearing in mind that this assumption is only valid for the solutions with relatively high

conductivity (i.e., high ionic strength) and at low current densities, this approach may be used in many CO_2 corrosion scenarios.

34.3.3.3 Initial and boundary conditions

The solution of Eq. (34.48), as a transient partial differential equation, requires the proper initial and boundary conditions to be specified. At the initial time ($t = 0$) it can be assumed that the well-mixed solution comes into contact with the metal surface. Hence, the concentrations of chemical species throughout the diffusion layer are constant, known values, defined by the chemical equilibria of the solution as discussed in Section 34.2.

At the bulk solution ($x = \delta$) the concentration of chemical species remains unchanged at all times ($t \geq 0$). Therefore, a Dirichlet type boundary condition can be defined for the bulk solution based on the known concentration of species identical to the initial conditions.

The boundary condition at the metal/solution interface is the Neumann boundary condition of defined fluxes and includes all the electrochemical reaction rate calculations. For an electroactive chemical species, the flux at the metal/solution boundary is equal to the rate of the corresponding electrochemical reactions. For an electroactive species, i involved in j electrochemical reactions, the flux at the metal surface can be described through Eq. (34.60).

$$N_i\big|_{x=0} = -\sum_j \frac{s_{ij} i_j}{n_j F} \tag{34.60}$$

The current−potential relationships, used to calculate the rate of electrochemical reactions, can be found in Table 34.5. The negative sign in Eq. (34.60) represents a sign convention, where cathodic currents are presumed negative and anodic currents are positive. For the electrochemical reactions shown in Table 34.2, the species on the left hand side are represented with a negative stoichiometric coefficient (S_{ij}) and the ones on the right hand side, with positive numbers.

Similar to the homogeneous chemical reaction, Eq. (34.60) can be transformed into a matrix notation to include all the electroactive species:

$$\begin{bmatrix} N_{Fe^{2+}_{aq}}\big|_{x=0} \\ N_{H^{+}_{aq}}\big|_{x=0} \\ N_{H_2CO_{3,aq}}\big|_{x=0} \\ N_{HCO^{-}_{3,aq}}\big|_{x=0} \\ N_{CO^{2-}_{3,aq}}\big|_{x=0} \\ N_{OH^{-}_{aq}}\big|_{x=0} \end{bmatrix} = \begin{bmatrix} 1 & 0 & 0 & 0 & 0 \\ 0 & -1 & 0 & 0 & 0 \\ 0 & 0 & -1 & 0 & 0 \\ 0 & 0 & 1 & -1 & 0 \\ 0 & 0 & 0 & 1 & 0 \\ 0 & 0 & 0 & 0 & 1 \end{bmatrix} \times \begin{bmatrix} i_{Fe}/2F \\ i_{H^+}/F \\ i_{ca}/F \\ i_{bi}/F \\ i_w/F \end{bmatrix} \tag{34.61}$$

For nonelectroactive species the flux at the metal surface is zero:

$$N_i\big|_{x=0} = 0 \tag{34.62}$$

Eq. (34.60) and (34.62) can be applied to describe the mass transfer for all chemical species at the metal surface. The electric potential inside the solution may also be specified through the electroneutrality constraint via Eq. (34.59) (or Poisson's equation) similar to that in the governing equations.

Considering the governing equations, the initial conditions, and the boundary conditions discussed so far, this system of equations is fully specified if the potential at the metal surface (E_{app} in Table 34.5) is known so that the rate of electrochemical reactions can be calculated. That is common in case of electroanalytical measurements (e.g., potentiodynamic sweep) where electrode potential is the controlled parameter. However, in corrosion rate predictions this parameter (E_{app} = corrosion potential) is generally not known a priori. In that case, an additional relationship is required—the charge conservation at the metal surface. All the cathodic (reduction) currents are balanced by the anodic (oxidation currents), meaning that the net current resulting from all j electrochemical reactions is equal to zero (i.e., there is no need for an externally "applied" current i_{app}). The charge conservation can be mathematically expressed as Eq. (34.63).

$$i_{app} = 0 = \sum_j i_j \tag{34.63}$$

Table 34.10 summarizes all the relevant mathematical equations required to develop a comprehensive mathematical model as discussed in this section.

34.3.3.4 Numerical solution

The mathematical equations as summarized in Table 34.10 form a set of nonlinear, coupled, partial differential equations to be solved numerically. With the simple one-dimensional geometry spanning from the metal surface toward the solution, typical for uniform corrosion rate calculations, the finite difference method can be used to solve the equations. This method is commonplace in mathematical modeling of electrochemical systems [95–97] and have been discussed in detail elsewhere [85,98].

The partial differential equations are discretized using Taylor's series approximations, resulting into a set of algebraic equations. These equations can further be transformed into a matrix format for convenience. The final solution can then be obtained through various solution algorithms such as Neman's "BAND" open source code where the coefficient matrix is developed and further solved by LU decomposition method [85,98].

In the numerical solution of this set of non-linear differential equations an explicit time integration approach is sometimes preferred over the implicit methods for simplicity. However, the nonlinear expressions in the electromigration and chemical reaction terms, as well as the nonlinear boundary conditions related to electrochemical

Table 34.10 Summary of equations used in the comprehensive mathematical model

Electrode surface boundary	
$N_i = -\sum_j \frac{s_{ij} i_j}{n_j F}$	for all electro active species
$N_i = 0$	for all non-electro active species
$\sum_i z_i C_i = 0$	
$i_{app} = 0 = \sum_j i_j$	for unknown electrode potential case
Diffusion layer	
$\frac{\partial C_i}{\partial t} = -D_i \frac{\partial}{\partial x}\frac{\partial C_i}{\partial x} - \frac{\partial}{\partial x}\left(\frac{z_i D_i F C_i}{RT}\frac{\partial \phi}{\partial x}\right) + v_x \frac{\partial C_i}{\partial x} + R_i$	for all species
$\sum_i z_i C_i = 0$	
Bulk boundary and initial condition	
$C_i = C_i^b$	for all species
$\Phi = 0$	

rate calculations, are often the cause of instability of calculations when an explicit approach was used. A simple remedy is using iterations; although this approach is mathematically simple, it can be computationally demanding, because it requires a very fine spatial and temporal resolution to ascertain the convergence of the calculation.

A more robust approach is based on the use of implicit methods including Taylor series expansion for linear approximation of the nonlinear terms [2,85]. Although this approach adds more complexity to the mathematical treatment, it improves stability of the calculations and enables handling of a variety of different imposed environmental conditions during corrosion rate calculations. Furthermore, to decrease the computational errors, higher order approximations of the nonlinear terms can be used along with an iterative scheme.

Depending on the simulation goals, one may prefer either of these approaches. For example, if the purpose of the model is to predict a highly transient, short time, response of the system such as potentiodynamic sweeps, a high temporal resolution is already required to achieve a reasonable accuracy and therefore, a simple explicit scheme would be suitable. On the other hand, if the model is developed to predict long-term corrosion rates, using much larger time steps is the only feasible approach that would keep the computational time reasonable, which must be done by using implicit methods coupled with higher order approximations and iterative procedures.

An example of comprehensive mechanistic models for CO_2 corrosion of steel was developed by Nešić et al. [2,23,24]. In addition to current/potential calculation for each electrochemical reaction, these models can provide the concentration profile of the chemical species throughout the diffusion layer. Fig. 34.6 illustrates an example of such calculations at pH 6 and 1 bar (14.5 psi) CO_2 [2].

34.3.3.5 Summary

The comprehensive mathematical models reflect the state of the art in the mechanistic understanding of the uniform CO_2 corrosion. These models allow the simultaneous consideration of all the main physiochemical processes in CO_2 corrosion, with each process being described through basic theoretical laws. The comprehensive models have all the key advantages of the elementary mechanistic models and much more. The ability of these models to incorporate any number of homogeneous and surface reactions provides a strong platform for corrosion rate predictions for more realistic industrial conditions. In particular, the effect of homogeneous chemical reactions and the complex interaction of the chemical species in the solution is an essential aspect of CO_2 corrosion that remains unresolved in the elementary models, making it an exclusive feature of the comprehensive mechanistic models. Of course, there are still many knowledge gaps with respect to various aspects of CO_2 corrosion; yet these models have the necessary flexibility to include new/improved understanding of physiochemical processes as they are uncovered. With such a strong theoretical foundation, these models are well suited to serve as a basis for future developments. Challenges would include modeling for higher temperatures and pressures, prediction of localized corrosion, effect of oil/water wetting, effect of corrosion inhibitors, etc.

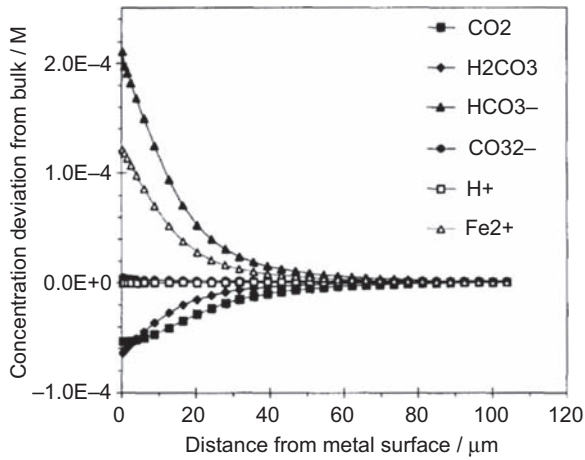

Figure 34.6 Concentration profile of electroactive species at pH 6, 1 bar CO_2 (14.5 psi), 20°C (68°F), pipe with 0.1 m diameter, and 1 m/s flow velocity.
Reproduced with permission from NACE International, Houston, TX. All rights reserved. S. Nešić, M. Nordsveen, R. Nyborg, A. Stangeland, Paper 40 presented at CORROSION 2001, Houston, TX. © NACE International 2001.

However, the comprehensive mathematical models come with their own "price tag." These models are mathematically and computationally more demanding and are more complicated to construct. The numerical solution algorithms, computational stability, and the calculation time are among the aspects that one needs to consider when developing these types of models.

34.4 Effect of the corrosion product layer

The CO_2 corrosion is often accompanied by corrosion product layer formation at the metal surface. In the simplest case, at the conditions typical for CO_2 corrosion in transmission lines, this corrosion product layer is dominated by the iron carbonate deposit. The protectiveness, mechanical properties, and physical properties of this precipitated layer are affected by numerous parameters such as water chemistry, environmental conditions such as temperature and fluid flow, steel composition, and microstructure, etc. [99−107].

The precipitation/dissolution of iron carbonate as demonstrated through the following heterogeneous chemical equilibrium (Reaction 34.64) is mathematically described via Eq. (34.65), where K_{sp} is the iron carbonate solubility product constant [102].

$$Fe^{2+} + CO_3^{2-} \rightleftharpoons FeCO_{3(s)} \tag{34.64}$$

$$K_{sp} = C_{Fe^{2+}} C_{CO_3^{2-}} \tag{34.65}$$

If the product of the concentration of the dissolved ions exceeds the saturation limit (K_{sp}), the formation of iron carbonate precipitation is thermodynamically favored. This porous deposit may affect the corrosion rate through two main mechanisms:

- Limiting the rate of mass transfer of the chemical species toward and away from the metal surface, as a physical barrier.
- Reducing the rate of electron transfer reactions by blocking a portion of the metal surface, making them unavailable as reaction sites.

The formation of a protective iron carbonate layer in CO_2 corrosion of steel can be discussed from both a thermodynamic and a kinetic point of view [99]. A thermodynamic indicator for the precipitation process is described by the extent of departure from equilibrium Eq. (34.64), represented by "saturation value" (S_{FeCO_3}) defined as:

$$S_{FeCO_3} = \frac{C_{Fe^{2+}} C_{CO_3^{2-}}}{K_{sp}} \tag{34.66}$$

However, although a high saturation value is an indication of iron carbonate layer formation, it does not represent the protectiveness quality of the deposit. The latter is mainly determined by the properties of the iron carbonate layer, such as density,

porosity, and adherence to the metal surface, which are greatly affected by kinetics of iron carbonate precipitation [99,106]. Furthermore, the protectiveness of the corrosion product layer can be influenced by various chemical and mechanical removal processes [103,108,109].

A more representative measure for the quality of a protective iron carbonate layer would therefore have to include the kinetic aspects of the layer deposition, in addition to the thermodynamic feasibility of the layer formation. In this regard, van Hunnik et al. [99] introduced the so-called "scaling tendency" parameter—described by Eq. (34.67)—as a practical measure to assess the protectiveness and sustainability of an iron carbonate layer [99,100,110]. The authors suggest that, the formation of an iron carbonate layer does not completely stop the corrosion process, which in turn causes the existing corrosion product layer to detach from the metal surface [99,111]. This process, known as "film undermining" [25], affects the adherence, density, and porosity of the corrosion product layer and ultimately its protectiveness.

$$ST = \frac{R_{FeCO_{3(s)}}}{CR} \tag{34.67}$$

Based on the aforementioned discussion, a scaling tendency of ST $\gg$ 1 suggests that the undermining is overpowered by the rapidly forming iron carbonate precipitate, creating a dense protective layer. On the other hand, a scaling tendency of ST $\ll$ 1 represents the case where the undermining is much faster than the formation of the corrosion product layer; therefore, only a porous and nonprotective layer may be formed, even at high saturation values [25,110].

The precipitation rate of iron carbonate in Eq. (34.67) can be described by an expression in general form of Eq. (34.68) [112].

$$R_{FeCO_{3(s)}} = \frac{A}{V} f(T) g(S_{FeCO_3}) \tag{34.68}$$

where $f(T) = e^{\left(A - \frac{B}{RT}\right)}$ represents the temperature dependence of the rate constant based on Arrhenius' law with constants A and B to be determined empirically. The precipitation rate dependence on saturation value is accounted for by the $g(S_{FeCO_3})$ function that is defined by the mechanism of the precipitation/dissolution reaction. For an elementary reaction this function can be theoretically expressed as Eq. (34.69) [112].

$$g(S_{FeCO_3}) = K_{sp}(S_{FeCO_3} - 1) \tag{34.69}$$

This equation is similar to what was proposed by Sun and Nesic [113] indicating that the precipitation reaction follows a first-order reaction kinetics. Alternative forms of the function $g(S_{FeCO_3})$, such as the ones introduced by van Hunnik et al. [99] and Johnson and Tomson [107], may suggest a more complex mechanism for this reaction (Table 34.11). However, the lack of mechanistic justification of these precipitation rate equations reduces them to semiempirical expressions with all of their intrinsic limits. A summary of the expressions for precipitation rate proposed by the abovementioned references is provided in Table 34.11.

Table 34.11 Summary of the precipitation rate expressions.

Reference	$f(T)$	$g(S_{FeCO_3})$	K_{sp}
Johnson and Tomson [107]	$e^{\left(54.8-\frac{-123000}{RT}\right)}$	$K_{sp}\left({S_{FeCO_3}}^{0.5}-1\right)^2$	$e^{\left(-36.22-\frac{-30140}{RT}\right)}$
van Hunnik et al. [99]	$e^{\left(52.4-\frac{-119800}{RT}\right)}$	$K_{sp}(S_{FeCO_3}-1)\left(1-{S_{FeCO_3}}^{-1}\right)$	Not specified
Sun and Nesic [113]	$e^{\left(21.3-\frac{-64851.4}{RT}\right)}$	$K_{sp}(S_{FeCO_3}-1)$	[102]

Reprinted with permission from A. Kahyarian, M. Singer, S. Nesic, Modeling of uniform CO_2 corrosion of mild steel in gas transportation systems: a review, Journal of Natural Gas Science and Engineering 29 (2016) 530−549.

In the case of elementary mechanistic models, the effect of a protective iron carbonate layer can be accounted for by introducing an additional mass transfer resistance layer and the blocking effect of the iron carbonate deposit on the charge transfer rates. Under such circumstances, the current density is calculated using Eq. (34.33), whereas a composite mass transfer coefficient should be used when calculating the limiting current densities (Eq. 34.34), to account for the effect of corrosion product layer on the mass transfer rate of the electroactive species. The composite mass transfer coefficient for each species ($k_{comp.}$) can be obtained via Eq. (34.70).

$$\frac{1}{k_{comp.}} = \frac{1}{k_m} + \frac{1}{k_d} \tag{34.70}$$

The term k_m in Eq. (34.70) is the mass transfer coefficient inside the solution similar to that discussed in Section 34.3.2.2, whereas k_d, is the mass transfer coefficient for species i inside the porous corrosion product layer. That is essentially the diffusion through a porous medium with porosity of ε, tortuosity of τ, and the thickness of δ_l, which can be described as:

$$k_d = \frac{\varepsilon \tau D_i}{\delta_l} \tag{34.71}$$

The effect of slow carbon dioxide hydration reaction on carbonic acid limiting current density can be included in the calculations in a similar fashion as described in Section 34.3.2.2. However, the mathematical relationships, such as the one derived by Nešić et al. [76], need to be reworked with a different set of boundary conditions to accommodate for the effect of the corrosion product layer.

While this approach can be used to properly reflect the effect of corrosion product layer, the aforementioned intrinsic shortcoming of the elementary mechanistic models remains unresolved—i.e. disregarding the homogeneous chemical reactions in the diffusion layer. Additionally, although being simple to implement, this approach further requires that the thickness (δ_l) and porosity (ε) of a protective iron carbonate layer to be specified before any corrosion rate calculation (Eq. 34.71). As these parameters are usually not known, an additional empirical correlation is needed, relating the properties (protectiveness) of a protective iron carbonated layer to environmental conditions [23].

Using an approach similar to that discussed above, the comprehensive mechanistic models can also be adapted to account for the effect of a precipitated corrosion product layer. An additional mass transfer barrier can be included in these models by considering a new boundary at the corrosion product layer interface ($x = \delta_l$), with the boundary conditions based on the known flux of chemical species. To account for mass transfer through a porous media, with a porosity ε, the Nernst–Planck equation is rewritten as [2,23]:

$$\frac{\partial(\varepsilon C_i)}{\partial t} = -\nabla \cdot \left(\varepsilon^{3/2} N_i\right) + \varepsilon R_i \tag{34.72}$$

where at the $x > \delta_l$ distance away from the steel surface, where there is no iron carbonate layer, the porosity ε is equal to one. Furthermore, all electrochemical rate expressions (current densities) are modified by multiplying with surface porosity ε, to account for the surface blocking effect. Although these models benefit from accurate surface concentration calculations and account for the homogeneous chemical reactions, the distribution of porosity in the precipitating iron carbonate layer still needs to be predefined. In a simplistic approach it could be described by an empirical function in the same way as it is done for the elementary models [23].

Using a more comprehensive approach, Nešić et al. presented a model for calculation of porosity distribution in the iron carbonate layer [24,80]. The authors proposed that the porosity could be calculated using a mass balance for the solid iron carbonate precipitate as:

$$\frac{\partial \varepsilon}{\partial t} = -\frac{M_{FeCO_3}}{\rho_{FeCO_3}} R_{FeCO_3} - CR\frac{\partial \varepsilon}{\partial x} \tag{34.73}$$

where the first term is related to precipitation kinetics (Eq. 34.68) and the second (convective-like) term arises from the undermining effect as described earlier. This approach is equivalent to using the concept of scaling tendency but one that is based on local concentrations at the steel surface and in the porous iron carbonate layer, rather than bulk concentrations. With this approach, the porosity is treated as an additional variable in calculations and its distribution through the diffusion layer can be obtained by solving Eq. (34.73) simultaneously with Eq. (34.72) for all the other unknown variables (e.g., concentration of species).

Fig. 34.7 shows the comparison of the calculated results with the experimental data obtained in the study by Nešić et al. [25]. The estimated profile of corrosion product

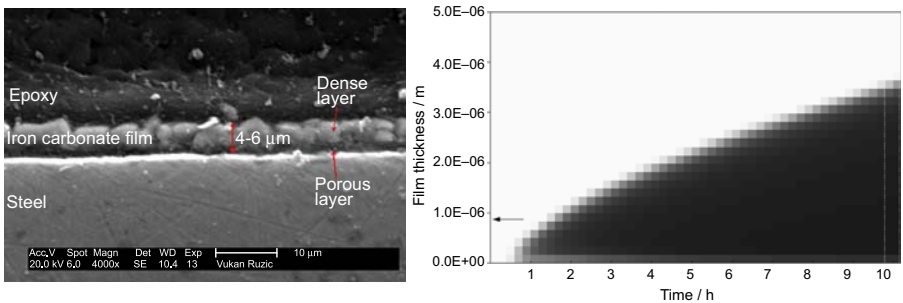

Figure 34.7 SEM image of the corrosion product layer cross section formed after 10 h at $T = 80°C$ (176°F), pH = 6.6, $P_{CO_2} = 0.54$ bar (7.8 psi), ferrous ion concentration of 250 ppm, and $v = 1$ m/s. The graph at right shows the calculated porosity profile along the film thickness of the iron carbonate layer depicted in different shades of gray in similar conditions where white corresponds to $\varepsilon = 1$ and black is $\varepsilon = 0$.

layer porosity shows good qualitative agreement with the SEM image, where a dense precipitate is found with the part closer to the metal surface appearing to be more porous. However, as discussed by the authors, the estimated corrosion product layer thickness lacks accuracy at some of the conditions, which could be due to imprecise iron carbonate deposition kinetics or a removal processes via mechanical destruction as well as chemical dissolution [103,108,109], which are not considered in that model [25].

34.5 Summary

Uniform CO_2 corrosion can now be considered a mature topic in the context of corrosion science and engineering. The understanding of the underlying physiochemical processes enables construction of mechanistic models of varying complexity, which can be successfully used to aid our understanding of the complex interplay between different parameters and to predict the corrosion rates. Furthermore, they may serve as a repository of the current knowledge on the topic, as well as a solid platform for building in new effects as they are discovered and understood.

While we have come a long way in the past few decades, plenty of challenges lie ahead. Modeling the effect of high pressure (close to and above the critical point for CO_2) and high temperature (above 100°C) is currently being addressed. Complexities arising from multiphase flow affecting water wetting in oil transportation lines and water condensation in wet gas lines are another major modeling challenge. The effect of H_2S, organic acids, nonideal solutions (due to very high concentrations of dissolved solids), scaling, underdeposit corrosion, erosion–corrosion, and corrosion inhibition are some of the new frontiers in CO_2 corrosion modeling. A number of research groups around the world are currently working on many of these issues, and as the understanding matures, it will find its way into the mechanistic CO_2 corrosion models of the future.

A special mention should be given to modeling of localized CO_2 corrosion. This is the ultimately challenging topic lying ahead of us, because there is no single cause or mechanism governing localized CO_2 corrosion. However, some progress has been made and the solid foundation built in terms of mechanistic CO_2 corrosion models will serve as a good platform for expanding these models to address localized corrosion.

Nomenclature

Symbol	Definition
A	Surface area (m^2)
C_i	Concentration of species i (M)
C_i^b	Concentration of species i at bulk (M)
C_i^s	Concentration of species i at metal surface (M)
CR	Corrosion rate (mm/year)

Continued

Symbol	Definition
D_i	Diffusion coefficient of species i (m^2/s)
$D_{i,ref}$	Diffusion coefficient of species i at reference temperature (m^2/s)
E	Electrode potential (V)
E_{0_j}	Standard potential of reaction j (V)
F	Faradays constant (C/mol)
ΔH_j	Enthalpy of reaction j (kJ/mol)
i_j	Current density of reaction j (A/m^2)
i_{corr}	Corrosion current density (A/m^2)
i_{net}	Net current density (A/m^2)
i_{ct}	Charge transfer−controlled current density (A/m^2)
i_{lim}	Limiting current density (A/m^2)
i_{app}	Applied current density (A/m^2)
K_j	Equilibrium constant of reaction j
K_{sp}	Solubility product constant (M^2)
k_{0_j}	Rate constant of electrochemical reaction j
$k_{0_{j,ref}}$	Rate constant of electrochemical reaction j at reference temperature
K_H^0	Henry's constant at water saturation pressure (M/bar)
k_m	Mass transfer coefficient in solution ($mol/s \cdot m^2 \cdot M$)
k_d	Mass transfer coefficient in porous deposit ($mol/s \cdot m^2 \cdot M$)
$k_{comp.}$	Composite mass transfer coefficient ($mol/s \cdot m^2 \cdot M$)
k_f	Forward reaction rate constant
k_b	Backward reaction rate constant
Mw_{Fe}	Molecular weight of Fe (kg/kmol)
$M_{\mathrm{FeCO_3}}$	Molecular weight of $FeCO_3$ (kg/kmol)
n_j	Number of transferred electrons in electrochemical reaction j
N_i	Flux of species i ($mol/m^2 \cdot s$)
R	Universal gas constant ($J/K \cdot mol$)
PF	Poynting correction factor
$P_{\mathrm{CO_{2(g)}}}$	Partial pressure of CO_2 (bar)
P_{tot}	Total pressure (bar)
P	Pressure (bar)

Symbol	Definition
P_{CO_2S}	Saturation pressure of CO_2 (bar)
P_{ws}	Saturation pressure of water (bar)
R_i	Reaction rate of species i (M/s)
Re	Reynolds number
S_{FeCO_3}	Saturation value
Sc	Schmitt number
Sh	Sherwood number
ST	Scaling tendency
s_{ij}	Stoichiometric coefficient of species i in reaction j
T	Temperature (K)
T_{ref}	Reference temperature (K)
t	Time (s)
u_i	Mobility of species i (m/s)
V	Volume (m^3)
$\widetilde{V_m}$	Molar partial volume of $CO_{2(aq)}$
v_x	Velocity along x axis (m/s)
x	Distance from metal surface (m)
z_i	Charge of ion i
α_j	Transfer coefficient of electrochemical reaction j
δ	Diffusion layer thickness (m)
δ_d	Diffusion layer thickness (m)
δ_r	Reaction layer thickness (m)
δ_l	Corrosion product layer thickness (m)
ε	Dielectric constant
ε	Porosity
μ	Water viscosity (kg/s·m)
μ_{ref}	Water viscosity at reference temperature (kg/s·m)
ρ_{Fe}	Density of iron (kg/m^3)
ρ_w	Density of water (kg/m^3)
ρ_{FeCO_3}	Density of iron carbonate (kg/m^3)
υ	Kinematic viscosity (m^2/s)
ϕ	Electric potential inside liquid (V)

Continued

Symbol	Definition
ϕ_s	Electric potential inside liquid at the metal surface (i.e., ohmic drop) (V)
φ_{CO_2}	Fugacity coefficient of $CO_{2(g)}$
τ	Corrosion product tortuosity
ω	Angular velocity (rad/s)

References

[1] C. de Waard, D.E. Milliams, Prediction of carbonic acid corrosion in natural gas pipelines, in: Intern. Extern. Prot. Pipes, 1975. F1-1−F1-8.

[2] M. Nordsveen, S. Nešić, R. Nyborg, A. Stangeland, A mechanistic model for carbon dioxide corrosion of mild steel in the presence of protective iron carbonate films − part 1: theory and verification, Corrosion 59 (2003) 443−456.

[3] C. de Waard, D.E. Milliams, Carbonic acid corrosion of steel, Corrosion 31 (1975) 177−181.

[4] L.G.S. Gray, B.G. Anderson, M.J. Danysh, P.R. Tremaine, Mechanisms of carbon steel corrosion in brines containing dissolved carbon dioxide at pH 4, in: CORROSION, 1989. Paper No. 464.

[5] L.G.S. Gray, B.G. Anderson, M.J. Danysh, P.R. Tremaine, Effect of pH and temperature on the mechanism of carbon steel corrosion by aqueous carbon dioxide, in: CORROSION, 1990. Paper No. 40.

[6] E. Remita, B. Tribollet, E. Sutter, V. Vivier, F. Ropital, J. Kittel, Hydrogen evolution in aqueous solutions containing dissolved CO_2: quantitative contribution of the buffering effect, Corrosion Science 50 (2008) 1433−1440.

[7] T. Tran, B. Brown, S. Nešić, Corrosion of mild steel in an aqueous CO_2 environment − basic electrochemical mechanisms revisited, in: CORROSION, 2015. Paper No. 671.

[8] A. Kahyarian, B. Brown, S. Nesic, Mechanism of cathodic reactions in acetic acid corrosion of iron and mild steel, Corrosion 72 (2016) 1539−1546.

[9] A. Kahyarian, M. Singer, S. Nesic, Modeling of uniform CO_2 corrosion of mild steel in gas transportation systems: a review, Journal of Natural Gas Science and Engineering 29 (2016) 530−549.

[10] T. Tran, B. Brown, S. Nešic, Investigation of the electrochemical mechanisms for acetic acid corrosion of mild steel, Corrosion 70 (2014) 223−229.

[11] Y. Zheng, B. Brown, S. Nešic, Electrochemical study and modeling of H_2S corrosion of mild steel, Corrosion 70 (2014) 351−365.

[12] J. Kittel, F. Ropital, F. Grosjean, E.M.M. Sutter, B. Tribollet, Corrosion mechanisms in aqueous solutions containing dissolved H_2S. Part 1: characterisation of H_2S reduction on a 316L rotating disc electrode, Corrosion Science 66 (2013) 324−329.

[13] S. Olsen, CO_2 corrosion prediction by use of the Norsok M-506 model − guidelines and limitations, in: CORROSION, 2003. Paper No. 623.

[14] S. Olsen, A.M. Halvorsen, P.G. Lunde, R. Nyborg, CO_2 corrosion prediction model − basic principles, in: CORROSION, 2005. Paper No. 551.

[15] A.M. Halvorsen, T. Sontvedt, CO_2 corrosion model for carbon steel including wall shear stress model for multiphase flow and limits for production rate to avoid mesa attack, in: CORROSION, 1999. Paper No. 42.
[16] A. Dugstad, L. Lunde, K. Videm, Parametric study of CO_2 corrosion of carbon steel, in: CORROSION, 1994. Paper No. 14.
[17] C. de Waard, U. Lotz, Prediction of CO_2 corrosion of carbon steel, in: CORROSION, 1993. Paper No. 069.
[18] C. de Waard, U. Lotz, A. Dugstad, Influence of liquid flow velocity on CO_2 corrosion: a semi-empirical model, in: CORROSION, 1995. Paper No. 128.
[19] C. de Waard, U. Lotz, D.E. Milliams, Predictive model for CO_2 corrosion engineering in wet natural gas pipelines, Corrosion 47 (1991) 976−985.
[20] C. de Waard, L.M. Smith, B.D. Craig, Influence of crude oils on well tubing corrosion rates, in: CORROSION, 2003. Paper No. 629.
[21] S. Nešić, H. Li, J. Huang, D. Sormaz, An open source mechanistic model for CO_2/H_2S corrosion of carbon steel, in: CORROSION, 2009. Paper No. 572.
[22] S. Nešić, J. Postlethwaite, S. Olsen, An electrochemical model for prediction of corrosion of mild steel in aqueous carbon dioxide solutions, Corrosion 52 (1996) 280−294.
[23] S. Nešić, M. Nordsveen, R. Nyborg, A. Stangeland, A mechanistic model for CO_2 corrosion with protective iron carbonate films, in: CORROSION, 2001. Paper No. 040.
[24] S. Nešić, J. Lee, V. Ruzic, A mechanistic model of iron carbonate film growth and the effect on CO_2 corrosion of mild steel, in: CORROSION, 2002. Paper No. 237.
[25] S. Nešić, K.L.J. Lee, A mechanistic model for carbon dioxide corrosion of mild steel in the presence of protective iron carbonate films − part 3: film growth model, Corrosion 59 (2003) 616−628.
[26] G. Schmitt, B. Rothmann, Studies on the corrosion mechanism of unalloyed steel in oxygen-free carbon dioxide solutions part I. Kinetics of the liberation of hydrogen, Werkstoffe Und Korrosion 28 (1977) 816.
[27] Revised Release on the IAPWS Industrial Formulation 1997 for the Thermodynamic Properties of Water and Steam, The International Association for the Properties of Water and Steam, Lucerne, Switzerland, August 2007.
[28] D. Li, Z. Duan, The speciation equilibrium coupling with phase equilibrium in the H_2O-CO_2-NaCl system from 0 to 250°C, from 0 to 1000 bar, and from 0 to 5 molality of NaCl, Chemical Geology 244 (2007) 730−751.
[29] Z. Duan, R. Sun, C. Zhu, I.-M. Chou, An improved model for the calculation of CO_2 solubility in aqueous solutions containing Na^+, K^+, Ca^{2+}, Mg^{2+}, Cl^-, and SO_4^{2-}, Marine Chemistry 98 (2006) 131−139.
[30] Z. Duan, D. Li, Coupled phase and aqueous species equilibrium of the $H_2O-CO_2-NaCl-CaCO_3$ system from 0 to 250°C, 1 to 1000 bar with NaCl concentrations up to saturation of halite, Geochimica et Cosmochimica Acta 72 (2008) 5128−5145.
[31] W.L. Marshall, E.U. Franck, Ion product of water substance, 0−1000°C, 1-10,000 bars New International Formulation and its background, Journal of Physical and Chemical Reference Data 10 (1983) 295−304.
[32] A.G. Dickson, C. Goyet (Eds.), DOE Handbook of Methods for the Analysis of the Various Parameters of the Carbon Dioxide System in Sea Water, second ed., 1994.
[33] D.A. Palmer, R. Van Eldik, The chemistry of metal carbonate and carbon dioxide complexes, Chemical Reviews 83 (1983) 651−731.
[34] L. Korson, W. Drost-Hansen, F.J. Millero, Viscosity of water at various temperatures, The Journal of Physical Chemistry 73 (1969) 34−39.

[35] J.E. Garcia, Density of Aqueous Solutions of CO_2, Lawrence Berkeley National Laboratory, 2001.
[36] C.L. Yaws, The Yaws Handbook of Vapor Pressure: Antoine Coefficients, second ed., 2015.
[37] Z. Duan, R. Sun, An improved model calculating CO_2 solubility in pure water and aqueous NaCl solutions from 273 to 533 K and from 0 to 2000 bar, Chemical Geology 193 (2003) 257−271.
[38] J. Oddo, M. Tomson, Simplified calculation of $CaCO_3$ saturation at high temperatures and pressures in brine solutions, Journal of Petroleum Technology 34 (1982) 1583−1590.
[39] R.F. Weiss, Carbon dioxide in water and sea water: the solubility of a non-ideal gas, Marine Chemistry 2 (1974) 203−215.
[40] T.H. Maren, L.C. Garg, The rates of hydration of carbon dioxide and dehydration of carbonic acid at 37°, Biochimica et Biophysica Acta 261 (1971) 70−76.
[41] D.M. Kern, The hydration of carbon dioxide, Journal of Chemical Education 37 (1960) 14−23.
[42] A.L. Soli, R.H. Byrne, CO_2 system hydration and dehydration kinetics and the equilibrium CO_2/H_2CO_3 ratio in aqueous NaCl solution, Marine Chemistry 78 (2002) 65−73.
[43] W. Stumm, J.J. Morgan, Aquatic Chemistry: Chemical Equilibria and Rates in Natural Waters, 1995.
[44] M.F. Mohamed, A.M. Nor, M.F. Suhor, M. Singer, Y.S. Choi, Multiphase Technology, Water chemistry for corrosion prediction in high pressure CO_2 environments, in: CORROSION, 2011. Paper No. 375.
[45] B. Meyssami, M.O. Balaban, A.A. Teixeira, Prediction of pH in model systems pressurized with carbon dioxide, Biotechnology Progress 8 (1992) 149−154.
[46] R. Nyborg, Overview of CO_2 corrosion models for models for wells and pipelines, in: CORROSION, 2002. Paper No. 233.
[47] S. Nešić, J. Postlethwaite, M. Vrhovac, CO_2 corrosion of carbon steel − from mechanistic to empirical modelling, Corrosion Reviews 15 (1997) 211−240.
[48] V.R. Jangama, S. Srinivasan, A computer model for prediction of corrosion of carbon steels, in: CORROSION, 1997. Paper No. 318.
[49] B.F.M. Pots, R.C. John, I.J. Rippon, M.J.J.S. Thomas, S.D. Kapusta, M.M. Grigs, et al., Improvements on de Waard-Milliams corrosion prediction and applications to corrosion management, in: CORROSION, 2002. Paper No. 235.
[50] R. Nyborg, P. Andersson, M. Nordsveen, Implementation of CO_2 corrosion models in a three-phase fluid flow model, in: CORROSION, 2000. Paper No. 048.
[51] S.D. Kapusta, B.F.M. Pots, I.J. Rippon, The application of corrosion prediction models to the design and operation of pipelines, in: CORROSION, 2004. Paper No. 633.
[52] S. Nešić, Key issues related to modelling of internal corrosion of oil and gas pipelines − a review, Corrosion Reviews 49 (2007) 4308−4338.
[53] R. Nyborg, Field data collection, evaluation and use for corrosivity prediction and validation of models, in: CORROSION, 2006. Paper No. 118.
[54] E. Dayalan, G. Vani, J.R. Shadley, S.A. Shirazi, E.F. Rybicki, Modeling CO_2 corrosion of carbon steels in pipe flow, in: CORROSION, 1995. Paper No. 118.
[55] E. Dayalan, F.D. de Moraes, J.R. Shadley, S.A. Shirazi, E.F. Rybicki, CO_2 corrosion prediction in pipe flow under $FeCO_3$ scale-forming conditions, in: CORROSION, 1998. Paper No. 51.
[56] J. Han, J.W. Carey, J. Zhang, Effect of sodium chloride on corrosion of mild steel in CO_2-saturated brines, Journal of Applied Electrochemistry 41 (2011) 741−749.

[57] J. Han, J. Zhang, J.W. Carey, Effect of bicarbonate on corrosion of carbon steel in CO_2 saturated brines, International Journal of Greenhouse Gas Control 5 (2011) 1680−1683.
[58] S. Rajappa, R. Zhang, M. Gopal, Modeling the diffusion effects through the iron carbonate layer in the carbon dioxide corrosion of carbon steel, in: CORROSION, 1998. Paper No. 026.
[59] M. Sundaram, V. Raman, M.S. High, D.A. Tree, J. Wagner, Deterministic modeling of corrosion in downhole environments, in: CORROSION, 1996. Paper No. 30.
[60] J. Han, J.W. Carey, J. Zhang, A coupled electrochemical-geochemical model of corrosion for mild steel in high-pressure CO_2-saline environments, International Journal of Greenhouse Gas Control 5 (2011) 777−787.
[61] Y. Zheng, J. Ning, B. Brown, S. Nesic, Electrochemical model of mild steel corrosion in a mixed H_2S/CO_2 aqueous environment, Corrosion 71 (2014) 316.
[62] A. Anderko, Simulation of $FeCO_3$/FeS scale formation using thermodynamic and electrochemical models, in: CORROSION, 2000. Paper No. 102.
[63] R. Zhang, M. Gopal, W.P. Jepson, Development of a mechanistic model for predicting corrosion rate in multiphase oil/water/gas flows, in: CORROSION, 1997. Paper No. 601.
[64] K. George, S. Nešić, C. de Waard, Electrochemical investigation and modeling of carbon dioxide corrosion of carbon steel in the presence of acetic acid, in: CORROSION, 2004. Paper No. 379.
[65] S.N. Esmaeely, B. Brown, S. Nesic, Verification of an Electrochemical Model for Aqueous Corrosion of Mild Steel for H_2S Partial Pressures up to 0.1 MPa, Corrosion 73 (2017) 144−154.
[66] M. Eisenberg, C.W. Tobias, C.R. Wilke, Ionic mass transfer and concentration polarization at rotating electrodes, Journal of the Electrochemical Society 101 (1954) 306−320.
[67] D.C. Silverman, Practical corrosion prediction using electrochemical techniques, in: Uhlig's Corros. Handb., John Wiley & Sons, Inc., 2011, pp. 1129−1166.
[67a] F.P. Berger, K.-F.F.-L. Hau, Mass transfer in turbulent pipe flow measured by the electrochemical method, International Journal of Heat and Mass Transfer 20 (11) (1977) 1185−1194.
[68] M.W.E. Coney, Erosion-Corrosion: The Calculation of Mass-transfer Coefficients, 1981.
[69] B. Poulson, Measuring and modelling mass transfer at bends in annular two phase flow, Chemical Engineering Science 46 (1991) 1069−1082.
[70] J. Wang, S.A. Shirazi, J.R. Shadley, E.F. Rybicki, E. Dayalan, A correlation for mass transfer coefficients in elbows, in: CORROSION, 1998. Paper No. 42.
[71] J. Wang, S.a Shirazi, A CFD based correlation for mass transfer coefficient in elbows, International Journal of Heat and Mass Transfer 44 (2001) 1817−1822.
[72] E.L. Cussler, Diffusion: Mass Transfer in Fluid Systems, Cambridge University Press, 1997.
[73] W.M. Haynes, CRC Handbook of Chemistry and Physics, 2009.
[74] B.R. Linter, G.T. Burstein, Reactions of pipeline steels in carbon dioxide solutions, Corrosion Science 41 (1999) 117−139.
[75] A.J. Bard, L.R. Faulkner, Electrochemical Methods : Fundamentals and Applications, John Wiley & Sons, Inc., 2001.
[76] S. Nešić, J. Postlethwaite, N. Thevenot, Superposition of diffusion and chemical reaction controlled limiting current-application to CO_2 corrosion, Journal of Corrosion Science and Engineering 1 (1995) 1−14.

[77] B.F.M. Pots, Mechanistic models for the prediction of CO_2 corrosion rates under multi-phase flow conditions, in: CORROSION, 1995. Paper No. 137.
[78] S. Turgoose, R.A. Cottis, K. Lawson, Modeling of electrode processes and surface chemistry in carbon dioxide containing solutions, in: Comput. Model. Corros., 1992, pp. 67−81. ASTM STP 1154.
[79] A. Więckowski, E. Ghali, M. Szklarczyk, J. Sobkowski, The behaviour of iron electrode in CO_2^- saturated neutral electrolyte—II. Radiotracer study and corrosion considerations, Electrochimica Acta 28 (1983) 1627−1633.
[80] S. Nešić, M. Nordsveen, R. Nyborg, A. Stangeland, A mechanistic model for carbon dioxide corrosion of mild steel in the presence of protective iron carbonate films—part 2: a numerical experiment, Corrosion 59 (2003) 489−497.
[81] B. Tribollet, J. Kittel, A. Meroufel, F. Ropital, F. Grosjean, E.M.M. Sutter, Corrosion mechanisms in aqueous solutions containing dissolved H_2S. Part 2: model of the cathodic reactions on a 316L stainless steel rotating disc electrode, Electrochimica Acta 124 (2014) 46−51.
[82] E. Remita, B. Tribollet, E. Sutter, F. Ropital, X. Longaygue, J. Kittel, et al., A kinetic model for CO_2 corrosion of steel in confined aqueous environments, Journal of the Electrochemical Society 155 (2008). C41−C45.
[83] J. Amri, E. Gulbrandsen, R.P. Nogueira, Numerical simulation of a single corrosion pit in CO_2 and acetic acid environments, Corrosion Science 52 (2010) 1728−1737.
[84] Z. Zhang, D. Hinkson, M. Singer, H. Wang, S. Nešić, A mechanistic model of top-of-the-line corrosion, Corrosion 63 (2007) 1051−1062.
[85] J. Newman, K.E. Thomas-Alyea, Electrochemical Systems, third ed., Wiley-Interscience, 2004.
[86] W.G. Cochran, The flow due to a rotating disc, Mathematical Proceedings of the Cambridge Philosophical Society 1 (1934) 365−375.
[87] S. Aravinth, Prediction of heat and mass transfer for fully developed turbulent fluid flow through tubes, International Journal of Heat and Mass Transfer 43 (2000) 1399−1408.
[88] J.T. Davies, Turbulence Phenomena, 1972, pp. 121−174.
[89] R.E. Zeebe, D. Wolf-Gladrow (Eds.), CO_2 in Seawater: Equilibrium, Kinetics, Isotopes, Elsevier, 2001.
[90] M. Eigen, Proton-transfer, acid-base catalysis, and enzymatic hydrolysis, Angewandte Chemie 3 (1964) 1−72.
[91] K.G. Schulz, U. Riebesell, B. Rost, S. Thoms, R.E. Zeebe, Determination of the rate constants for the carbon dioxide to bicarbonate inter-conversion in pH-buffered seawater systems, Marine Chemistry 100 (2006) 53−65.
[92] F.H. Stillinger, Proton transfer reactions and kinetics in water, Theoretical Chemistry, Advances and Perspectives 3 (1978) 177−234.
[93] N. Gavish, K. Promislow, Dependence of the dielectric constant of electrolyte solutions on ionic concentration: a microfield approach, Physical Review E − Statistical, Nonlinear, and Soft Matter Physics 94 (2016) 1−7.
[94] E. Cussler, Diffusion: Mass Transfer in Fluid Systems, third ed., Cambridge University Press, 2009.
[95] D. Coleman, R. White, D. Hobbs, A parallel-plate electrochemical reactor model for the destruction of nitrate and nitrite in alkaline waste solutions, Journal of the Electrochemical Society 142 (1995) 1152−1161.

[96] D. Fan, Modification of Newman's BAND(J) subroutine to multi-region systems containing interior boundaries: MBAND, Journal of the Electrochemical Society 138 (1991) 1688−1691.
[97] K.-M. Yin, T. Yeu, R.W. White, A mathematical model of electrochemical reactions coupled with homogeneous chemical reactions, Journal of the Electrochemical Society 138 (1991) 1051.
[98] J. Newman, Numerical solution of coupled, ordinary differential equations, Industrial and Engineering Chemistry Fundamentals 7 (1968) 514−517.
[99] E.W.J. van Hunnik, B.F.M. Pots, E.L.J.A. Hendriksen, The formation of protective $FeCO_3$ corrosion product layers in CO_2 corrosion, in: CORROSION, 1996. Paper No. 006.
[100] E. Gulbrandsen, Acetic acid and carbon dioxide corrosion of carbon steel covered with iron carbonate, in: CORROSION, 2007. Paper No. 322.
[101] J.-L. Crolet, N. Thevenot, A. Dugstad, Role of free acetic acid on the CO_2 corrosion of steels, in: CORROSION, 1999. Paper No. 24.
[102] W. Sun, S. Nešić, R.C. Woollam, The effect of temperature and ionic strength on iron carbonate ($FeCO_3$) solubility limit, Corrosion Science 51 (2009) 1273−1276.
[103] V. Ruzic, M. Veidt, S. Nešić, Protective iron carbonate films—part 3: simultaneous chemo-mechanical removal in single-phase aqueous flow, Corrosion 63 (2007) 758−769.
[104] M.B. Kermani, A. Morshed, Carbon dioxide corrosion in oil and gas production − a compendium, Corrosion 59 (2003) 659−683.
[105] D.H. Davies, T. Burstein, The effect of bicarbonate on the corrosion and passivation of iron, Corrosion 36 (1980) 416−422.
[106] A. Dugstad, Mechanism of protective film formation during CO_2 corrosion of carbon steel, in: CORROSION, 1998. Paper No. 31.
[107] M.L. Johnson, M.B. Tomson, Ferrous carbonate precipitation kinetics and its impact on CO_2 corrosion, in: CORROSION, 1991. Paper No. 268.
[108] V. Ruzic, M. Veidt, S. Nešsić, Protective iron carbonate films—part 2: chemical removal by dissolution in single-phase aqueous flow, Corrosion 62 (2006) 598−611.
[109] V. Ruzic, M. Veidt, S. Nešsić, Protective iron carbonate films—part 1: mechanical removal in single-phase aqueous flow, Corrosion 62 (2006) 419−432.
[110] W. Sun, S. Nesic, Basics revisited: kinetics of iron carbonate scale precipitation in CO_2 corrosion, in: CORROSION, 2006. Paper No. 365.
[111] B.F.M. Pots, E.L.J.A. Hendriksen, CO_2 corrosion under scaling conditions − the special case of top-of-line corrosion in wet gas pipelines, in: CORROSION, 2000. Paper No. 031.
[112] A.C. Lasaga, Kinetic Theory in the Earth Sciences, Princeton University Press, 1998.
[113] W. Sun, S. Nešić, Kinetics of corrosion layer formation: part 1 - iron carbonate layers in carbon dioxide corrosion, Corrosion 64 (2008) 334−346.